CZM-based FE numerical study on pull-out performance of adhesive bonded-in-rod (BiR) joints for timber structures

C. Bedon [a,*], V. Rajcic [b], J. Barbalic [b], N. Perkovic [b]

[a] Department of Engineering and Architecture, University of Trieste, 34127 Trieste, Italy
[b] Faculty of Civil Engineering, University of Zagreb, 10000 Zagreb, Croatia

ARTICLE INFO

Keywords:
Bonded-in Rods (BiR), service class
Polyurethane
Epoxy
Finite Element (FE) numerical modelling
Cohesive Zone Modelling (CZM)

ABSTRACT

Bonded-in-Rod (BiR) connections for timber structures are becoming rather popular solution, in place of other traditional fastening techniques. Besides, design rules and recommendations in support of safe and robust verification are still poor in existing standards. As such, the actual mechanical performance and load-bearing capacity – which is severely affected by a multitude of operational parameters – should be possibly addressed with the support of experimental investigations. In this paper, a Cohesive Zone Modelling (CZM) based, Finite Element (FE) numerical investigation is proposed for a total of 144 BiR joints characterized by various geometrical and mechanical properties, including grain orientation ($\alpha = 0°$ or $90°$), adhesive type (polyurethane or epoxy glue), diameter (d = 10, 14, 20 mm) and anchorage length of rods (L = 60, 100, 200, 400 mm) is presented. Most importantly, the attention is also focused on the analysis of service class effects / moisture content (9, 18 or 27 %) on the actual residual capacity of the examined joints, which is of paramount importance for safe design applications in timber structures. Based on validation of input model properties to past experimental results, the sensitivity of basic mechanical performance indicators for the examined BiR samples is discussed in the paper.

1. Introduction

In the past years, different types of mechanical fasteners for high-loaded structures have been investigated with different mechanical approaches. In most cases, the full load-carrying capacity of these joints cannot be used. Only 60–70 % of the applied loads will be transmitted through the joint into the supports or attached structural parts due to the low embedding stiffness and reduced load-carrying capacity when loaded under an angle to the grain. Bonded-in Rod (BiR) joints do not have such a low force transmission level within the connection when embedded in other composite materials. Considering the excellent properties of BiRs, like high stiffness, fire and corrosion resistance through embedment, these mechanical fasteners have a high potential in timber engineering with relation to economic, scientific and ecologic aspects. Besides, the BiR technique still needs to be improved for better quality control, lower assembling effort and of course to reduce the geometrical restrictions [1].

Extensive research studies, such as [2–23] among others, deal with bonded-in rods for connection systems, retrofitting and strengthening of existing structures. The mentioned research primarily relates to the basic behaviour laws, interfacial stress distributions and failure modes of axially loaded BiRs made of different materials (like steel, BFRP, CFRP, GFRP). To evaluate the mechanical performance of the bonded-in rods, different tests setups can be distinguished, the pull–pull tests and pull-compression test [23,24]. The former (pull-pull) test is the most used where the specimen is pulled axially in the longitudinal direction of the timber. Furthermore, a large number of experimental and theoretical studies (as shown in [22]) has been conducted to address guidelines for load-carrying capacity of bonded-in rods ([25–27] and others), as a function of the nominal rod diameter d (mm), the anchorage length l_b (mm), the shear strength of timber $f_{v,k}$ (N/mm^2) and its density ρ_k (kg/m^3) [19]. These models were developed for the BiR into sawn or glulam timber for both directions, parallel and perpendicular to the grain.

Due to the complexity and intrinsic uncertainty of BiR numerical models, compared to research through tests, extended computational investigations are not so widely present in the literature. A detailed state of the art overview is given in [28], while additional research can be found in [13,15,17,19]. So far, models have been developed for a wide range of material and geometrical properties, and most of existing research is based on similar approaches. Usually, simulations are

* Corresponding author.
E-mail address: chiara.bedon@dia.units.it (C. Bedon).

Accepted 19 October 2022

Table 1
Examples of bonded-in-rods in application in different consequence classes and relation to DSL and IL.

Consequence class	Description of consequence	Indicative qualification of consequence		Examples
		Loss of human life or personal injury*	Economic, social or environmental consequences *	
CC3	Higher	High	Very great	Grandstands, large buildings, e.g. a concert hall
CC2	Normal	Medium	Considerable	Residential and office buildings, small buildings
CC1	Lower	Low	Small	Agricultural buildings, buildings where people do not normally enter, such as storage buildings, etc.

* The consequence class is chosen based on the more severe of these two columns.

performed with three-dimensional (3D) Finite Element (FE) models, or "nite" elements using the general purpose "nite" element code. The typical model of a BiR specimen consists of three materials: wood, bondline and steel (or some other rod material). The wood and the steel parts usually are treated as linear elastic continua, while the bondline is modelled as a layer in which the shear stresses and the peel stress are nonlinear functions of the relative shear and normal displacements across the layer. The material parameters are most often assumed from literature, while the bondline model is implemented using an option of the FE-code allowing a user-defined material to be included in the analysis. The final material model results in an unsymmetrical tangential stiffness matrix of the equation system, so that the unsymmetrical equation solver, based on a standard Newton method, should be used to obtain an incremental solution [28].

The failure of BiR sample is assumed to take place at the adhesive layer. The input for the present bondline model is thus represented by the stress-slip performance of the adhesive layer in use, that is related to the fracture energy of adhesive, which is an important parameter for the prediction of the ultimate load of BiR. It is assumed that a stress-slip performance can be known for a small specimen in a stable pull-out test, which includes the strain-softening branch of the stress-slip curve. Then, it is possible to calibrate the input data for the bondline model in such a way that the test results can be reproduced in a FE numerical simulation [28]. It can be thus concluded that the bondline model is an efficient model for the adhesive itself but also for for the boundary layers on either side of it, if the failure mode in stable tests is equal to the failure mode expected for BiR sample. Furthermore, rods used in timber connections are usually profiled or threaded, but such irregularities, compared to a smooth rod of solid cross-section, are generally disregarded in models. Such a twofold effect can induce different responses for the bondline, compared to a smooth rod of the same diameter, and modifications can be noticed as well in terms of reduction of the axial stiffness [28].

This approach to BiR research is good because it enables an easier analysis of a large number of samples with different geometric and material characteristics. The models predict effects of absolute size and glued-in length on the nominal shear strength of bonded-in rods, which is a phenomenon known from test results of several research studies.

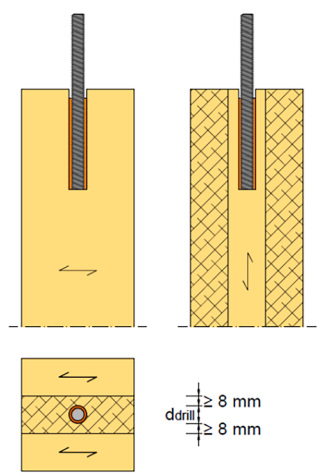

Fig. 2. Denotation of distances to cross-layers for bonded-in-rods.

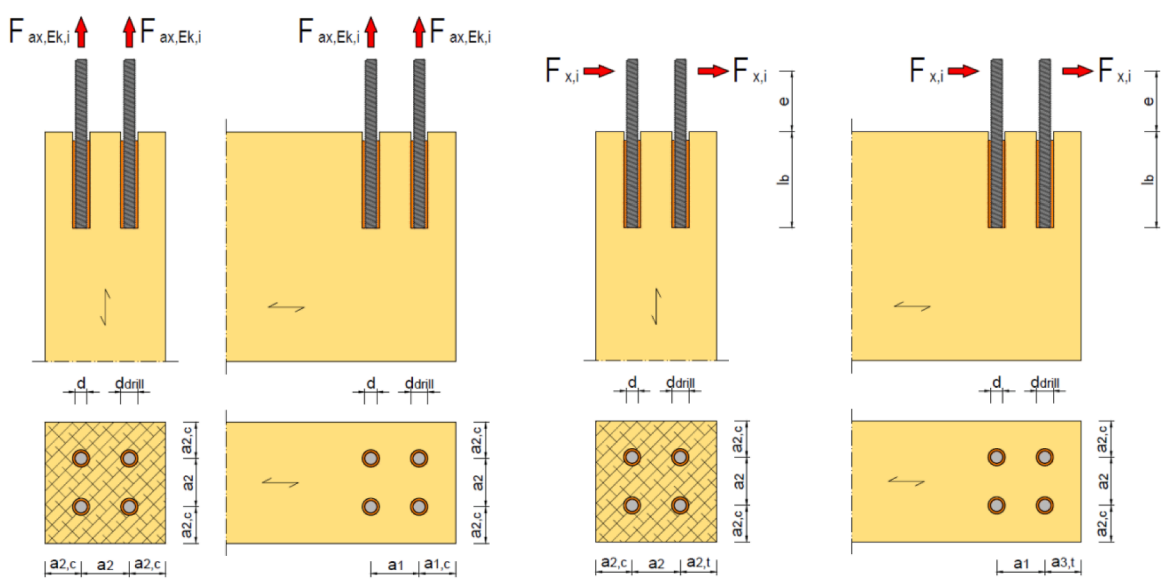

Fig. 1. Denotation of spacings and distances for bonded-in-rods.

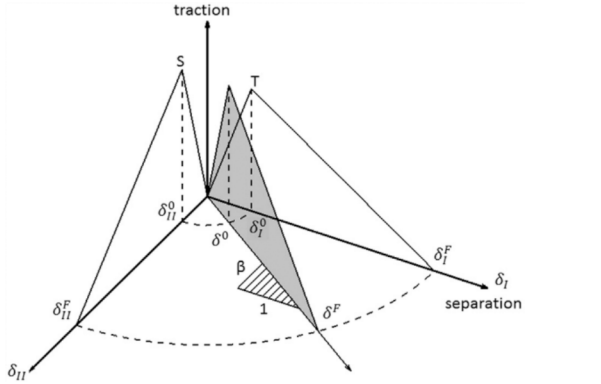

Fig. 3. The bi-linear traction separation laws for a mixed-mode loading analysis.

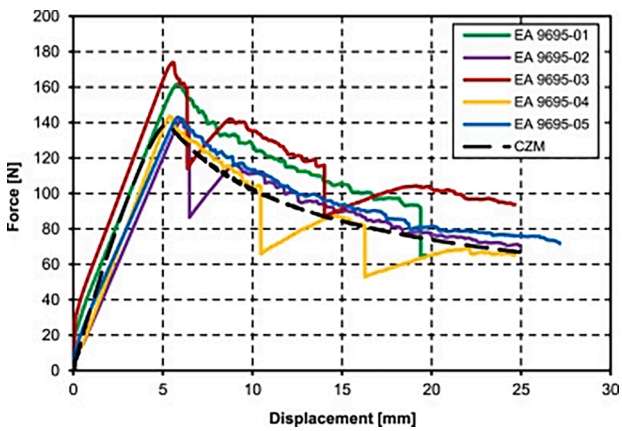

Fig. 4. Comparison between numerical (CZM) and experimental load–displacement curves obtained for DCB specimens (figure reproduced from [51]).

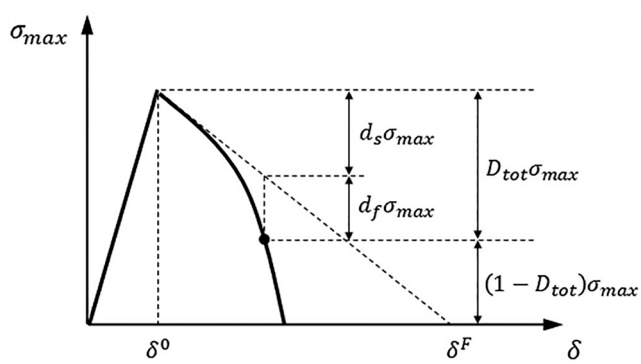

Fig. 5. The modified bi-linear traction-separation law for fatigue load (figure reproduced from [51]).

However, the influence of the material characteristics and the bond quality of the glued layer is rather difficult to define and quantify, without calibration in relation to experiments (See Table 1).

Although different, all the mentioned approaches show similarities in the calculation methods, because primarily agree that BiR load-carrying capacity increases with the increase of the anchorage length and the rod diameter [23]. These calculation methods are commonly used and validated in conjunction with linear elastic and mostly stiff adhesives [15] and consequently their prediction is highly depending on the loading direction regarding to the timber grain (longitudinal or

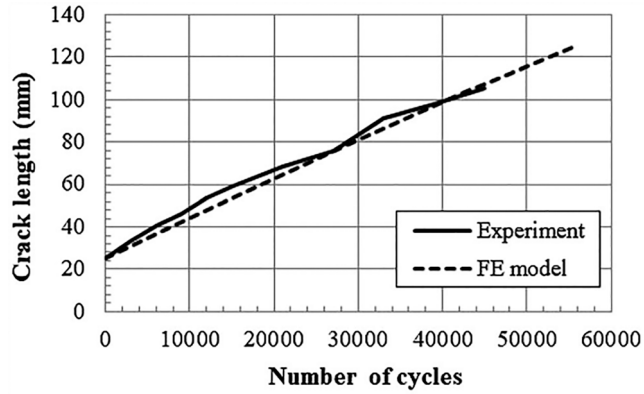

Fig. 6. Predicted and measured fatigue crack growth in a DCB specimen (figure reproduced from [51]).

perpendicular) [19]. However, as presented in [3] and [15], the load-bearing capacity of BiR is difficult to predict analytically due to the nonuniform distribution of the shear stresses along the anchorage length [29], especially in the case on long anchorages [19]. Furthermore, several important phenomena which affect the load-bearing capacity of BiR are not covered in enough extend by these approaches: the complexity of the orthotropic timber material behaviour as well as the failure within the adhesive layer (adhesive or cohesive).

Therefore, a need to develop a general predictive numerical approach based on the 3D continuum damage mechanics (CDM) modelling, capable of predicting both the pull-out response and the expected brittle failure modes, is still present. In this context, a FE model combining CDM and Cohesive Zone Modelling (CZM) approaches to simulate the progressive pull-out of rods bonded into timber is proposed and validated against experimental results published in [29]. An extended parametric study inclusive of 144 geometrical and operational configurations is presented and the effects of service class (with corresponding degradation in mechanical properties of bonding layers) on the load-carrying capacity of joints is discussed.

2. General design rules for BiR connections

Although in use for decades, BiR joints are not fully standardized, especially in Europe. Following in the large number of research's, European Committee for Standardization proposed some basic rules given in [30].

As far as the environment is concerned, bonded-in structural members are assigned to service classes 1 and 2. Also, structures are not subject to prolonged exposure to temperatures over 60 °C. Bonded-in-rods in load-bearing timber structures should be classified into consequence classes 1 to 3, according to the consequences of their failure as described according to [31]. In dependency of the consequence class the Design Supervision Level (DSL) and Inspection level (IL) of the bonded-in-rods should be chosen.

Principles of limit state design are based on axially loaded rods and laterally loaded rods. The load-carrying capacity of a connection made with bonded-in axially loaded rods shall be verified for the following failure modes: tension failure of the rod ("a"), compression (buckling) failure of the rod ("b"), failure of the adhesive in the bond-line and its bond to rod and timber ("c"), shear failure ("d") of the timber adjacent to the bond-line (where strain based approach to be included), splitting of the timber departing from the bonded-in-rods ("e") and timber failure ("f") of the member in the surrounding of the bonded-in-rod (e.g. net cross-section, or block-shear failure in a connection with several BiR). In the case of connections with several simultaneously acting rods, a uniform load distribution between rods is only possible if a ductile failure is achievable in the individual rods. Otherwise, a non-uniform force distribution between rods shall be assumed. Ductile behaviour of axially

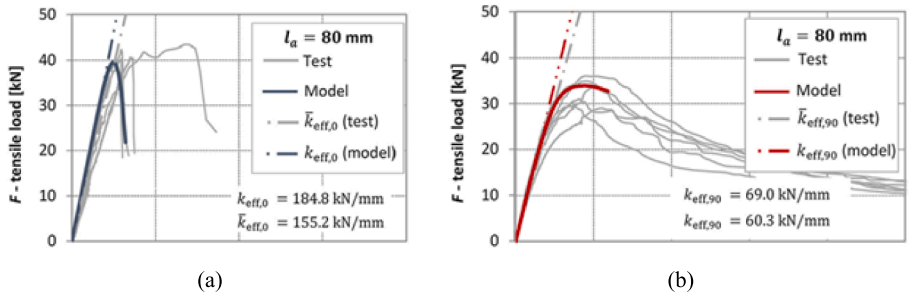

Fig. 7. Typical numerical and experimental predictions for glued-in-rods in CLT applications: rods arranged (a) parallel or (b) perpendicular to the grain of timber (figure reproduced from [51]).

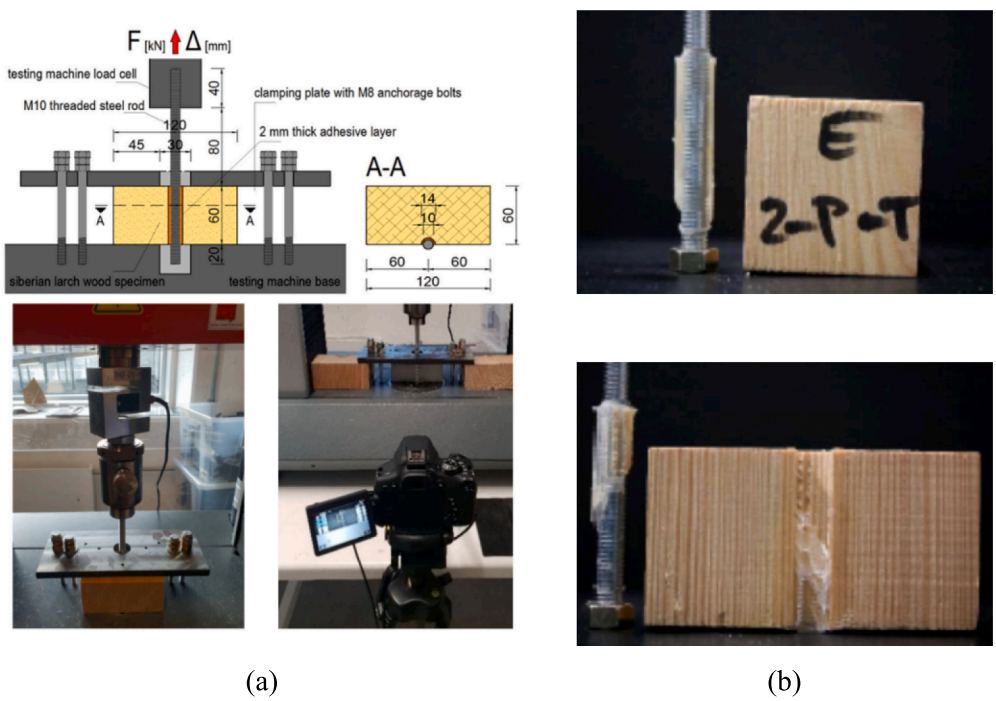

Fig. 8. Pull-out tests on BiR joints: (a) schematic view and details of setup (nominal dimension in mm) and (b) typical failure configuration (figures reproduced from [29] under CC-BY license agreement permission).

Table 2
Summary of basic properties for literature experimental samples taken into account in the numerical validation (with $L = 60$ mm, $d = 10$ mm, $t_{adh} = 2$ mm), $n = 5$ samples each.

Grain orientation	Glue	Moisture content [%]
$\alpha = 0°$	polyurethane, epoxy	9, 18, 27
$\alpha = 90°$	polyurethane, epoxy	9, 18, 27

loaded connections with BiRs is generally achieved if the tensile failure of the rod (failure mode "a"), which requires large deformations, occurs before the other possible failure modes. The force transmission between the adhesive and the rod shall be achieved mechanically and a possible adhesion should not be taken into account. The expressions given for failure mode "c" are based on the nominal diameter d of the rod. The expressions given for failure modes "d", "e" and "f" are based on the drill hole diameter d_{drill}. It should be noted that for most reinforcing bars used as ribbed rods, the outer diameter is about 10 % greater than the nominal diameter d.

The influence of load-duration and moisture on connections or reinforcements with bonded-in-rods should be considered using the modification factor k_{mod} and deformation factor k_{def} according to [32] for the strength properties of timber. Some conclusions about the increase or decrease of the modification factor are present, but due to the lack of research, they have not been accepted yet. The effects of moisture content changes in the timber shall be taken into account. The timber should be conditioned close to the final equilibrium moisture content. An expected average moisture content change of not more than 5 % is covered for bonded-in-rods with adhesive tested according to the [33]. It should be noted that in general, 5 % (for softwood) average moisture content change can be considered in Service class 1 and 2. For rods inserted perpendicular to the grain, the risk of splitting in the timber due to changes of moisture content should be considered. For the calculation of design value X_d of strength property, the partial factors γ_M shall be applied. For timber and bondline failure, the partial factor γ_M for material properties, also accounting for model uncertainties and dimensional variations is equal to 1.3. Partial factor $\gamma_{M,0}$ for failure of steel rod for resistance of cross-sections, whatever the class, is equal to1.1. Partial factor for failure of steel rod for resistance of cross-sections in tension to fracture, $\gamma_{M,2}$, has a reference value of 1.25.

Geometrical data may be taken from harmonized European Standards, product standards or drawings for execution and treated as nominal values. It shall be verified that the properties of the adhesive and its bond to rod and timber remain reliable within the designed

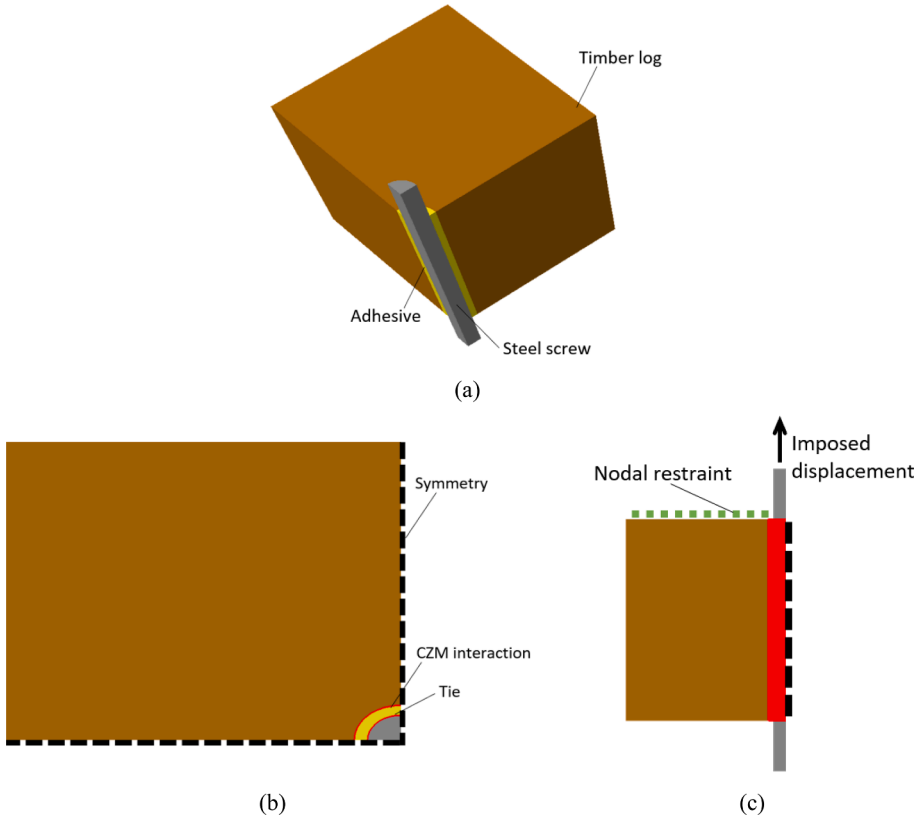

Fig. 9. Assembled FE model to reproduce the reference half-size BiR specimen (out-of-scale): (a) axonometric view; (b) top view and (c) side view (ABAQUS).

Table 3
Input material properties for constituent materials.

	E [GPa]	ν	ρ [kg/m^3]
Steel	200	0.3	7800
Timber ($\alpha = 0°$)	14.9	0.4	660
Timber ($\alpha = 90°$)	0.5	0.4	660
Polyurethane glue	0.295 (nominal), then variable (from test fitting)	0.336	1160
Epoxy glue	0.295 (nominal), then variable (from test fitting)	0.336	1160

temperature and moisture content ranges through-out the service life of the structure.

Rods may be bonded-into the following timber materials: glued laminated timber or glued solid timber according to [34], laminated veneer lumber according to [35], cross laminated timber according to [36] with edge-glued, ungrooved timber layers, solid wood panels according to [37]. The adhesive shall meet the performance requirements according to [33]. The bondline strength $f_{k1,k}$ shall be determined according to [33]. Rods should be profiled by metric thread or ribs. Threaded rods in the sense of this standard are threaded bolts that comply with EN ISO 898–1, with a nominal diameter of from 6 mm to 30 mm. It should be noted that Strength classes 4.8, 5.6 and 5.8 are recommended. For threaded rods made of stainless steel according to [38] property classes 45, 50, 60, 70 and 80 are recommended.

For durability the relevant provisions given in [31] and [32] apply. Rods should be corrosion-resistant or be protected against corrosion in accordance with EN 1995–1-1:2004 + A1:2008 clause 4.2 and EN 14592. The effect of chemical treatment of timber, or timber with high acidic content on the corrosion protection of fasteners should be considered in accordance with [39].

The bonded-in-rods nominal diameter d should not be less than 6 mm and not greater than 30 mm. The nominal stress area, A_s of threaded bonded-in-rods is defined according to [40]. The anchorage length, l_b should be greater than the minimum anchorage length, $l_{b,\min}$ determined by $\max(0.5d^2, 10d)$. The anchorage length of the bonded-in rod should not exceed 3000 mm and comply with a slenderness ratio of, l_b/d less than 110. The effective anchorage length, $l_{b,eff}$ should be determined by $\min(l_b, 40d, 1000\text{ mm})$. Minimum spacings and edge and end distances should be taken according to Fig. 1.

For axially loaded BiRs in the edge faces of laminated veneer lumber, cross laminated timber, solid wood panels and solid wood-based building products the distance from the drill hole to the next cross-veneer or cross-layer, respectively, should be not less than 8 mm according to Fig. 2.

To conclude, for rods inserted parallel to the grain and axially loaded rods, the connection in the bondline may be considered as quasi-rigid. The instantaneous slip modulus, K_{ser}, in N/mm per rod should be taken as $0.004d^{1.8}\rho_{mean}{}^{1.5}$, where ρ_{mean} is the mean density of the timber in kg/m^3.

For rods inserted perpendicular to the grain and laterally loaded, the instantaneous slip modulus per rod should be taken as $0.04d\rho_{mean}{}^{1.5}$. For rods inserted parallel to the grain and laterally loaded, the instantaneous slip modulus should be taken as $0.08d\rho_{mean}{}^{1.5}$. For BiRs inserted at an angle to the grain, finally, a linear interpolation should be applied.

3. Adhesive BiR connections and cohesive Zone modelling (CZM)

BiR connections are known to be advantageously bonded by adhesives and characterized by more uniform stress distribution along the joint, compared to conventional fastening techniques.

In ideal terms, it can be assumed that the maximum resistance capacity for a given set of material properties and geometrical parameters is equal to:

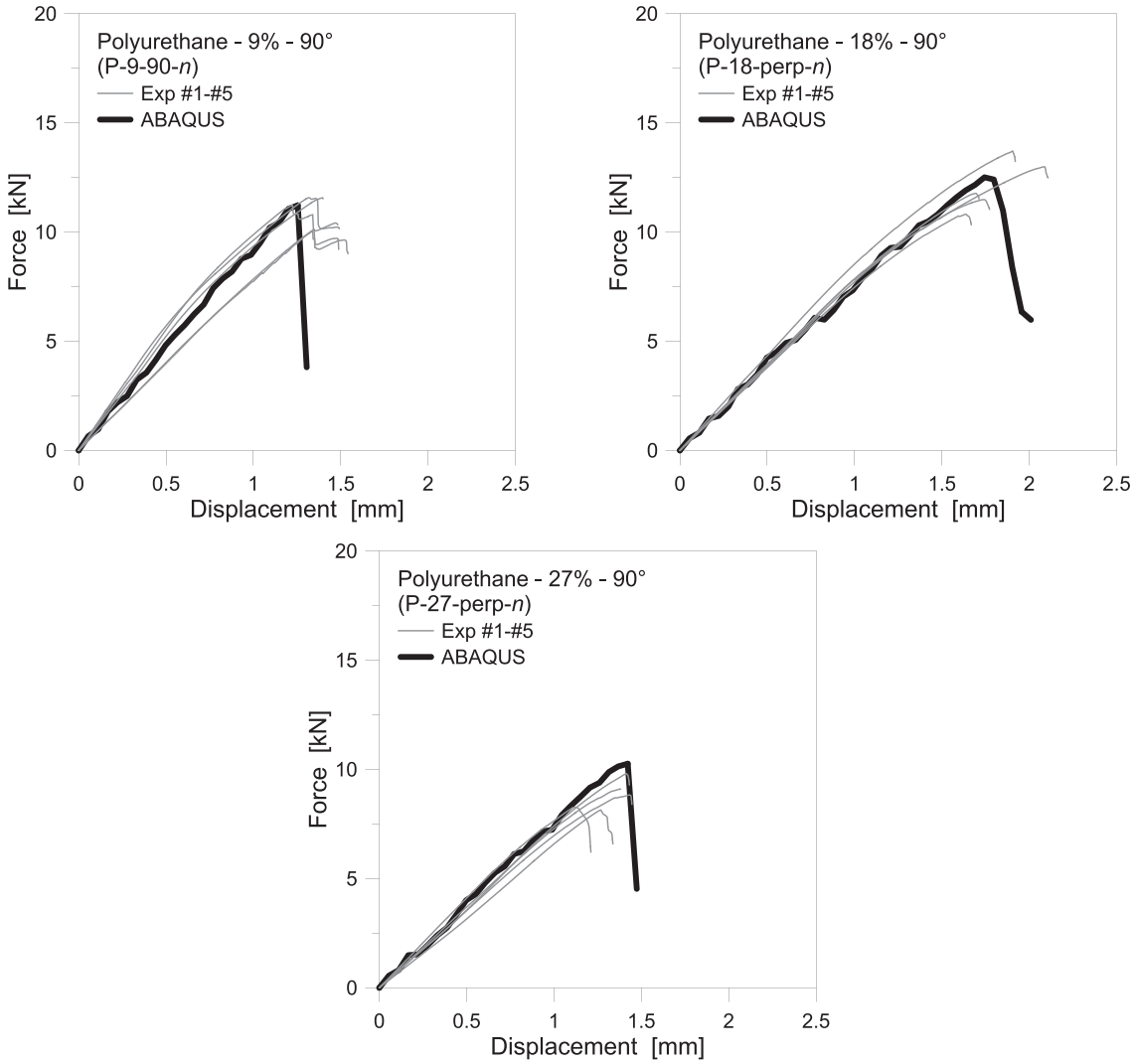

Fig. 10. Examples of FE model calibration for BiR connections (L = 60 mm, d = 10 mm, t_{adh} = 2 mm) – 9, 18 or 27 % moisture (ABAQUS).

$$F_{ax} \approx f_{mean} \pi d L \quad (1)$$

with f_{mean} the strength of wood, d the screw diameter and L the anchorage length.

Accordingly, the maximum stress in bondline can be estimated as:

$$\sigma_{max} \approx \frac{F_{ax}}{A_{bond}} \quad (2)$$

with A_{bond} the size of bondline.

However, a multitude of factors influence the quality of structural bonding between timber and metal components, giving evidence of different mechanical behaviours as well as structural performances. The stress distribution along the contact depends on the mechanical properties of the adhesives, moisture content and adherends, the geometry of the joint. Significant stress concentrations in adhesive joints can be avoided by applying a suitable adhesive, modulus of elasticity like the base material, ductile behaviour and high absorbent properties regardless of moisture level (good penetration into wood matrix).

In the typical FE model – possibly consisting of full 3D solid elements representative of the nominal specimens components – a key role should in fact be given to the mechanical description of materials (especially the adhesive and wood, so to account for possible cracking phenomena during the shear loading phase), as well as to cohesive surface interactions, being representative – within the CZM technique – of any kind of damage occurring at the interface between the adhesive layer and the bonded substrates. A special attention should be thus paid for the definition of major CZM input parameters, being responsible of severe (and even unreliable) effects on the corresponding FE estimations.

CZM is a damage mechanics-based numerical approach suitable for modelling crack initiation and propagation. The herein adopted technique is based on the original works of Barenblatt [41,42] and Dugdale [43] in the late 1950 s / early 1960 s, when the idea of a cohesion zone in front of the top of a crack was first proposed. Hilleborg et al. [44] proposed a numerical model that shows the function between traction and cracks separation. Another important study was presented by Needleman [45], where he demonstrated various polynomial and exponential functions for the definition of the law of traction separation. Typical bilinear traction separation laws for mixed-mode load analysis are shown in Fig. 3.

In the last years, CZM has advanced and set up a leading method for simulating the delamination of composite materials and adhesive joints for engineering applications [46–50]. Commercial FE platforms facilitated the use of this method for even complex geometries [51].

To determine the damage increase, CZM assumes a discontinuity in the displacement field [52]. Available shapes combined in this method and traction-separation laws are triangular [53], linear-parabolic [54], polynomial [55], exponential [56] and trapezoidal [57].

CZM approach has been successfully used by numerous authors for the simulation of delamination of CFRP materials as well as the

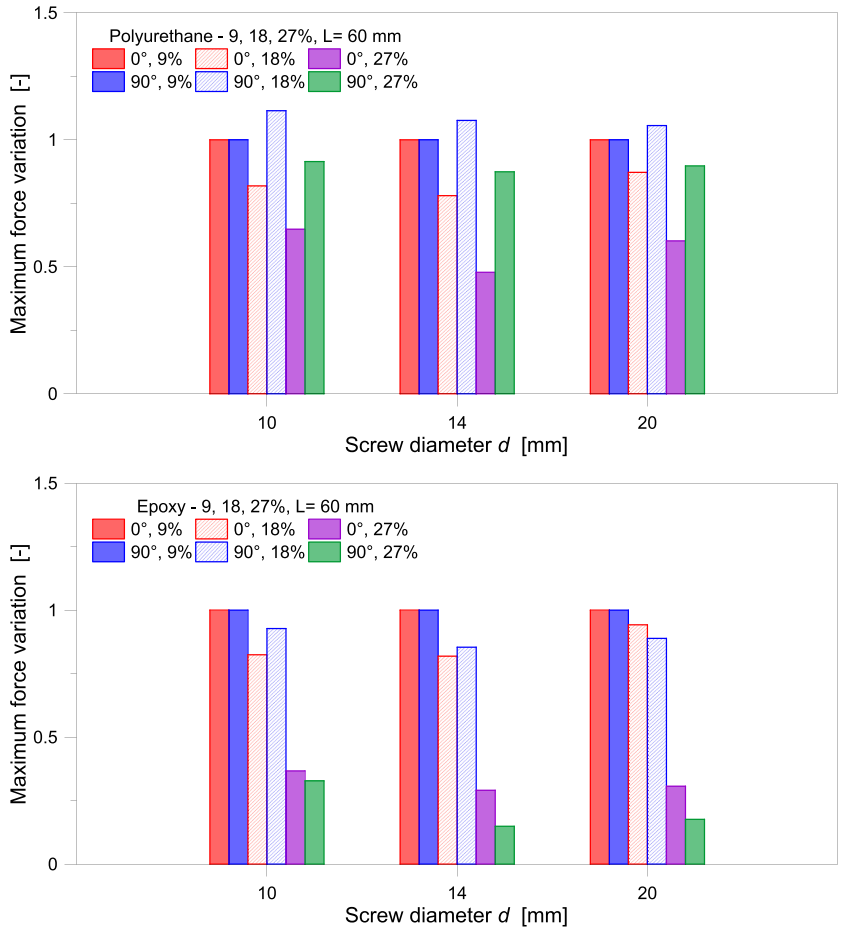

Fig. 11. Maximum force variation with screw diameter and moisture content (L = 60 mm, t_{adh} = 2 mm): (a) polyurethane or (b) epoxy (ABAQUS).

debonding initiation and growth of joints with metal and/or composite adherents. Dias et al. [58] used CZM to simulate the Mode I load in DCB samples. The trapezoid law of traction-separation was applied by De Moura et al. [59] to investigate Mode II load, both experimentally and numerically. Campilho et al. [60] studied the influence of input parameters and the shape of traction-separation law. The experimental work was confirmed by numerical simulations in [61] using the CZM approach to simulate Mode I, Mode II, and Mixed Mode I + II loads on composite bonded joints. A comparison of load–displacement curves is shown in Fig. 4 for a DCB sample.

Apart from simulating delamination and debonding under pseudo-static loading, CZM has also been used to investigate fatigue crack growth, which has been the subject of intense research in the last decade.

The idea which underpins the simulation of fatigue debonding growth is the modification of the bilinear traction-separation law by degrading the strength of the cohesive elements as a function of the applied load cycles [62,63]. For this purpose, a fatigue damage parameter is introduced which accounts exclusively for the damage due to fatigue loading. The concept of fatigue damage parameter and the way it is used to modify the bi-linear traction-separation law is illustrated in Fig. 5.

In general, validation of this kind of CZM-based numerical models necessarily requires a comparison with dedicated experimental results. Several authors have simulated fatigue debonding under Mixed-Mode I + II loading using a CTS specimen [64], SBS specimen [65], a Mixed-Mode I + II bending apparatus [66], and a CLS specimen [67]. Indicative results from the application of the CZM method to predict fatigue crack growth in the CLS specimen are given in Fig. 6.

As a method for failure simulation of adhesively bonded joints, CZM has certainly many advantages compared to other techniques. In the field of constructions, several literature studies can be found for various materials and systems. One of the popular areas of research using this method is joints in timber structural components [13,68–71]. Azinović et al. [13] indicated how the standard configuration of pull-pull test can be used for mechanical analysis and characterization of CZM input parameters. A similar modelling strategy was used for small-scale and full-scale timber-to-timber composite systems [68,69], where the contact region at the interface of steel threaded rod and the surrounding wooden elements was defined by CZM interaction. An intrinsic risk for those applications was detected in the potential occurrence and spread of local damage mechanisms (especially at the plane of symmetry of bars and constrained CZM nodes, if any) which could result in erroneous structural predictions for test specimens. In this sense, it could be required to analyze the full nominal geometry for specific configurations [69,70]. CZM modelling was finally used in [71] to capture damage mechanisms in timber-concrete composite joints Overall, the research showed great accuracy and benefit of the CZM method in the study of joints in wooden structures, see the examples in Fig. 7.

4. CZM-based FE modelling of BiR connections

4.1. Reference pull-out test results

Fig. 8 shows the geometry of the of pull-out test set-up studied experimentally by Barbalic et al. [29]. In total, 84 specimens were presented in extended series of experimental tests, with 72 “half-size” and 12 “standard”, full-size specimens. Among the half-size specimens,

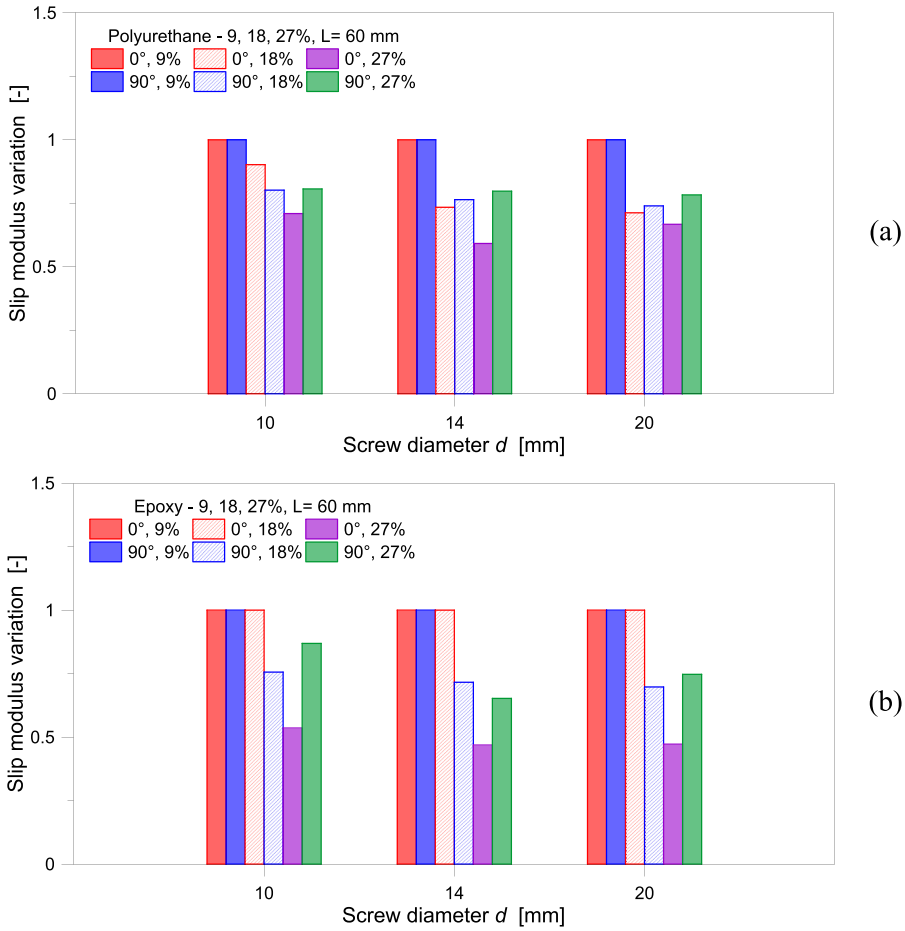

Fig. 12. Slip modulus variation with screw diameter and moisture content ($L = 60$ mm, $t_{adh} = 2$ mm): (a) polyurethane or (b) epoxy (ABAQUS).

36 samples were tested parallel and 36 perpendicular to the grains of timber. Furthermore, 12 full-size specimens tested to confirm the observed correlation between half-size and standard specimens.

Half-size specimens (with dimensions $B = 120 \times W = 60 \times L = 60$ mm) were drilled in their full height L with a concave-notch diameter equal to $d_h = 14$ mm. This hole was placed at the centre of the cross-section of each timber log, in order to introduce both the rod and the adhesive bond. Standard type specimens were characterized by double size ($B = 120 \times W = 120 \times L = 60$ mm) and prepared with a similar approach.

To get the results for the highest service class, Siberian larch (*Larix sibirica*) wood was used for the timber components [72]. After three weeks in a climate enclosure room with a controlled atmosphere, the moisture content was around 12 %. The measured average density was close to 600 kg/m^3, with a standard deviation of 25 kg/m^3.

One standard metrically threated steel rod with 8.8 strength, nominal diameter $d = 10$ mm and total length of 200 mm was bonded in each wooden specimen. The bonding effect was investigated with two different adhesive types, being represented by a two-component epoxy (KGK EPOCON '88) and a two-component polyurethane (LOCTITE PUREBOND CR 821). The bonding stage was performed under controlled laboratory conditions (9 % humidity in wood and room temperature of 20 °C).

The experiments reported herein comprised three artificial climates being selected as extreme examples of operational conditions for service class 1, 2 and 3. All test series were in fact performed at a constant temperature of 20 °C, with moisture content in wood in the order of 9 %, 18 % and 27 % respectively (Table 2). The stiffness and strength characteristics in short-term loading were thus investigated according to EN 15,274 recommendations [73]. Further, all tests were carried out based on the EN1382 provisions [74].

The anchorage length of 60 mm as well as rod diameter of 10 mm with an annular bond-line thickness of $t_{adh} = 2$ mm was kept fix for all the experimental samples, so that influence of other parameters could be considered [29].

4.2. *Finite Element numerical modelling*

The typical FE numerical model was developed in ABAQUS/Explicit [5], by taking into account the nominal geometry of "half-size" specimens and components represented in Fig. 8. More in detail, 8-node solid brick elements were used (C3D8R type from ABAQUS library). Symmetry conditions were taken into account to minimize the computational cost (Fig. 9).

To this aim, a variable mesh pattern was also used, with an edge size comprised between an average of 1–2 mm (glue bonding region) and up to 10–15 mm (external region of timber log), for a total of 15,000 solid elements and 43,000 DOFs in case of $L = 60$ mm setup. In the parametric study of Section 5.2, this total number of elements was increased with join size up to 45,000–50,000 bricks (for $L = 400$ mm). The typical FE analysis consisted of a dynamic simulation in ABAQUS/Explicit, with quasi-static application of deformations. Displacement-controlled analyses were carried out in accordance with the test setup of Fig. 8.

In this regard, a special care was spent in the FE modelling stage for some key parameters of models, namely boundaries and mechanical interactions between the involved components. Based on a preliminary analysis, the steel plates of experimental setup were disregarded. The top surface of timber log was rigidly restrained against vertical

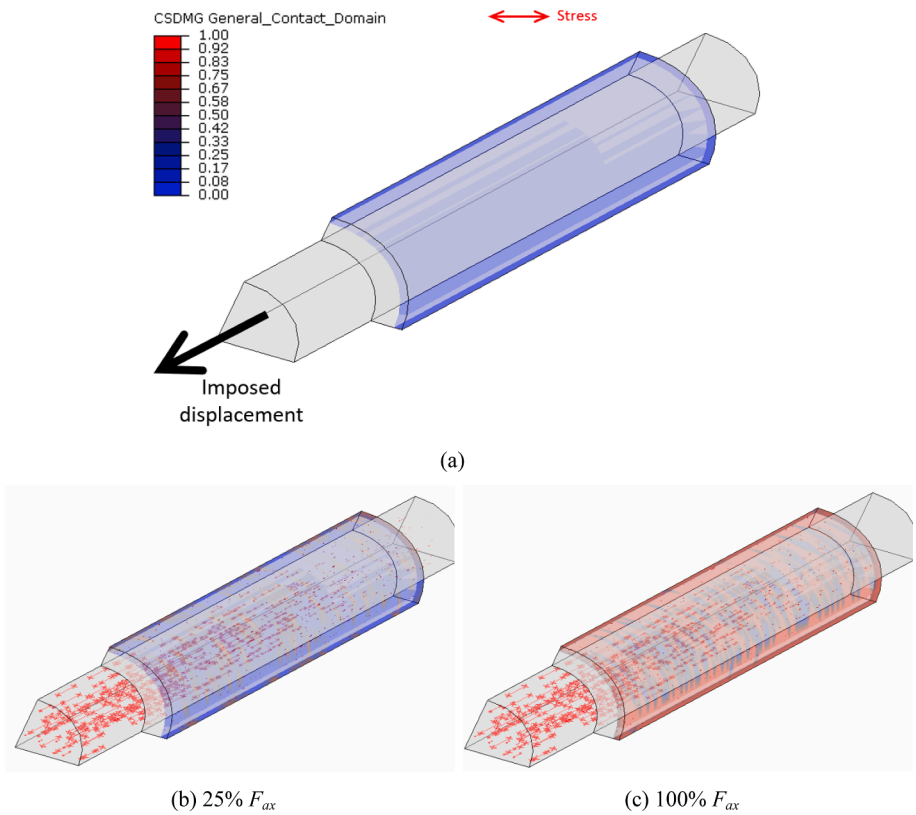

Fig. 13. Qualitative CZM damage and stress evolution in the bondline (and in screw): (a) unloaded sample; (b) 25 % of maximum axial load and (c) 100 % of axial maximum load (ABAQUS).

displacements. The steel rod was also properly restrained at the ends, so as to reproduce the experimental apparatus in Fig. 8, while the imposed vertical displacement was applied at the top end of the rod, and monotonically increased up to a maximum deformation of 2.5 mm. Such an amplitude was chosen based on the previous experimental observations, to exceed the ultimate load-bearing capacity of each sample. Regarding the materials in use, some mechanical simplifications were taken into account, and in particular (Table 3):

- for steel, a linear elastic constitutive law was defined, with input properties of 8.8 grade [1];
- for both the glue types in use (polyurethane or epoxy, in the following), an equivalent elastic–plastic constitutive law was separately defined, with input modulus of elasticity, resistance and damage parameters (if any) derived from technical data sheets of producers (Table 3). Successively, throughout the FE parametric analysis, the realistic calibration of mechanical properties was refined to capture the experimental load–displacement curves for the available test samples from [29] (Section 4.1);
- timber was described as an equivalent, linear elastic material with nominal elastic modulus (in the direction of interest) from [1–4]; in this manner, two different grain orientations were considered for the parametric analysis ($\alpha = 0°$ and 90°).

The mechanical interaction of model instances in Fig. 9 was ensured by appropriate constraints. A rigid "tie" connection was assigned at the rod-to-glue interface, thus preventing any kind of relative deformation between the involved nodes.

In the case of the glue-to-timber connection, otherwise, a CZM surface interaction was taken into account [6]. The initial stiffness parameters were set as "rigid", while cohesive damage initiation was based on the available resistance values for both the adhesive types in use. More in detail, CZM input was expressed in the form of tensile strength σ (stress perpendicular to the bond-line) and in-plane shear strengths τ_1 and τ_2. It is worth to remind that these strength values are representative of timber mechanical properties for the logs in use for the experimental program. As a result, they are no sensitive to variations in modifications of rod diameter or length [13]. Further, in accordance with [6], for the normal, longitudinal and radial stiffness terms K_{nn}, $K_{tt,1}$ and $K_{tt,2}$, the "default contact enforcement method" was taken into account. In terms of damage initiation, at the same time, the maximum nominal stress (MAXS) criterion was used [6].

Finally, key input parameters for damage progress were defined with a "linear" damage evolution law, which includes a linear degradation of mechanical CZM contact properties in use, with full degradation of residual stiffness for the CZM interaction at the first attainment of a given limit deformation d_u. In this regard, see also [13], it is important to note that the latter parameter represents a crucial input calibration process for FE calculations. It is in fact strictly related to stress/strain distributions in the load bearing components of investigated samples. Also, d_u can be hardly quantified and derived from experimental observations and measurements. As such, for the present study, d_u was separately calculated based on curve-fitting of load–displacement experiments from [29], based on iterative parametric numerical analyses to minimize the gap with experimental trends. Worth note that a similar calibration approach has been proposed in [13], with successful comparative analysis of CZM-based numerical models towards a wide set of experimental samples (60 in total). Moreover, whilst rather difficult to quantify, the d_u parameter has minimum effects on the maximum load-bearing capacity which can be expected from variably arranged BiR samples with identical mechanical properties but different geometric features (especially in terms of bonding length variations). On the other side, the d_u parameter has direct effects on the prediction of collapse mechanism, which for BiRs like in the present study is typically brittle [13,29]. In these conditions, the curve-fitting calibration of d_u to different experimental curves available in [29] for variations in grain

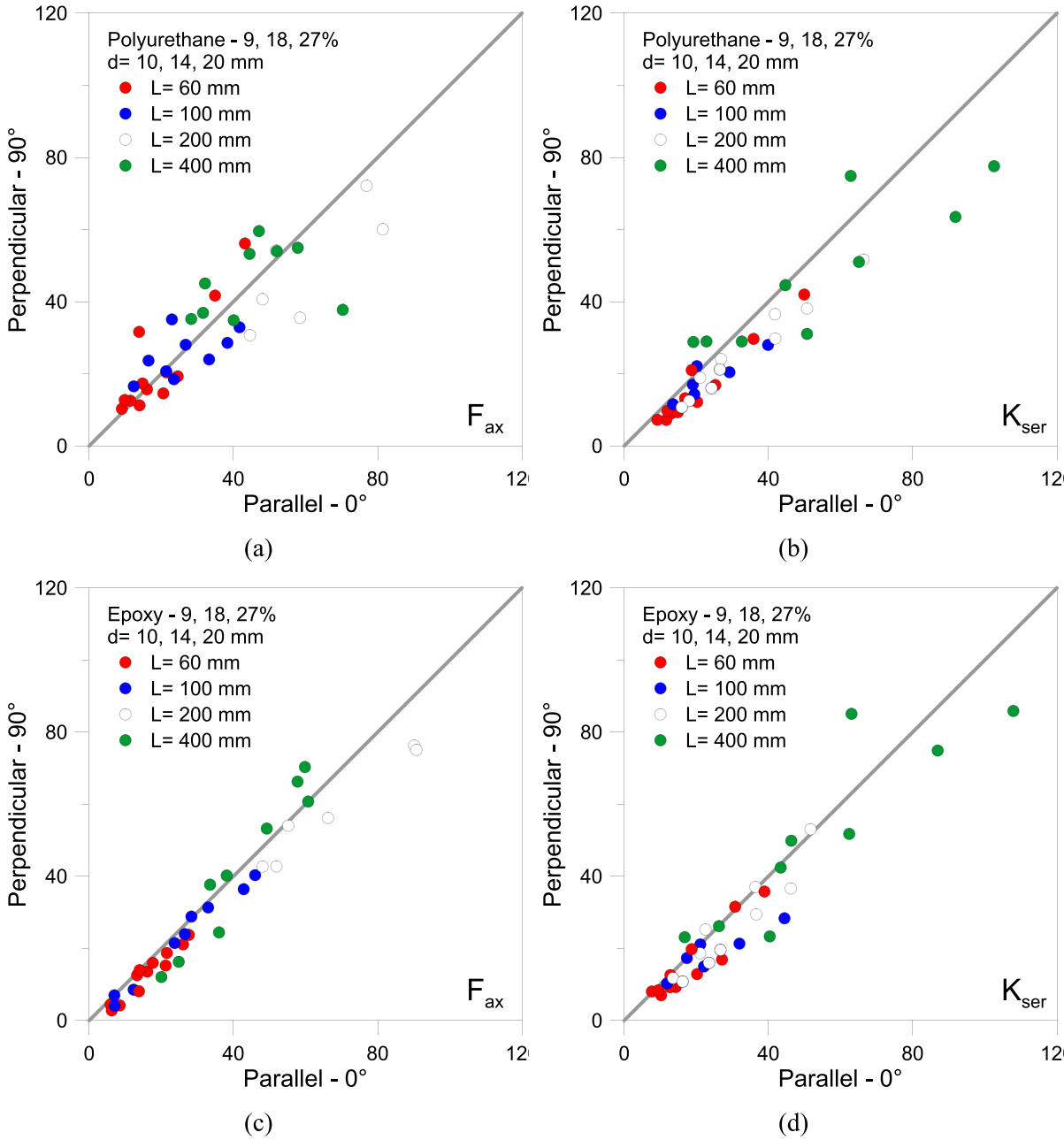

Fig. 14. Variation of ultimate axial force (F_{ax}) and slip modulus (K_{ser}) with grain orientation ($\alpha = 0°, 90°$) for the total set of 144 examined configurations: (a)-(b) polyurethane or (c)-(d) epoxy adhesive (ABAQUS).

orientation and moisture levels, whilst limited to a single rod diameter and bonding length, can be considered an efficient procedure to address the maximum force expected from the examined configurations.

5. Discussion of numerical results

The analysis of FE results included observations and comparisons in terms of (i) global load-bearing capacity for the examined BiR connections and (ii) local analysis of stress distribution and damage propagation at the CZM interface. Most importantly, as a function of the imposed vertical displacement, the attention was focused on:

- Maximum axial force sustained by each BiR connection (F_{ax});
- Initial stiffness (slip modulus K_{ser});
- Stress peaks and stress distribution along the adhesive bond (σ_{max});
- Evolution of damage parameters at the CZM interface (CSDMG damage parameter),
- Failure mechanism

5.1. Analysis of experimental configurations

Adhesive and CZM input parameters were calibrated based on the test setup in Fig. 8, that is $L = 60$ mm and $d = 10$ mm. The same input values, for the $t_{adh} = 2$ mm thick adhesive bond, were successively applied to the parametric investigation of BiR connections with increased diameter or anchorage length (and identical mechanical properties for materials and damage laws). Such a kind of calibration process follows the assumptions in Section 4.2, and especially for modifications in rod diameter and anchorage length, is able to capture the expected load-bearing capacity of examined BiR joints, with a

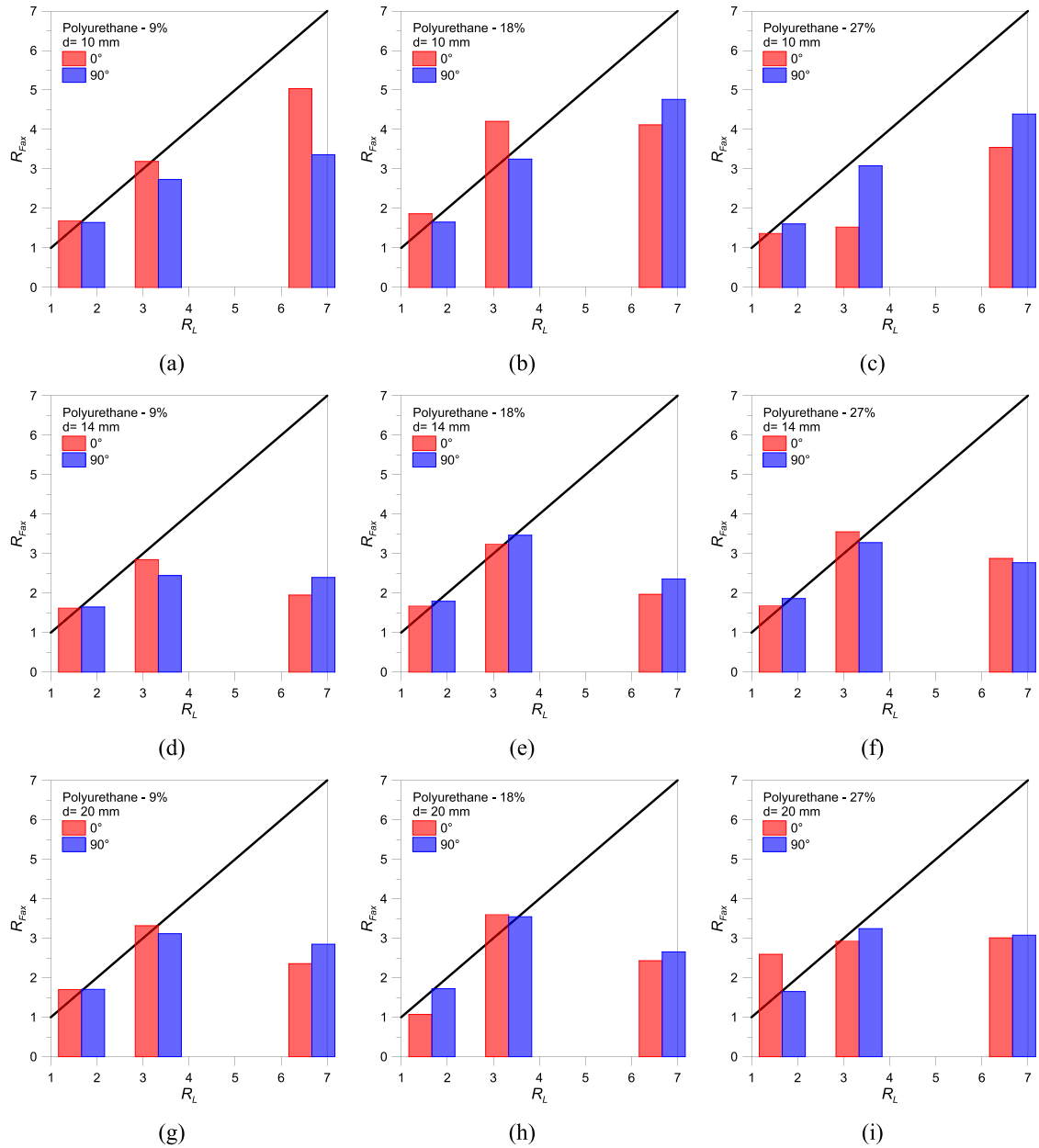

Fig. 15. Non-dimensional variation of maximum force (F_{ax}) with bond length, rod diameter and moisture content (polyurethane adhesive, ABAQUS).

particular attention to modifications in moisture content and grain orientation.

Fig. 10 shows a selection of load–displacement responses for each series of experiments recalled in Section 4.1 (see also Annex A). Numerical curves were grouped in items by moisture content, and then divided by type of glue and grain orientation. For each group of samples, the numerical analysis fits the trend of $n = 5$ different test samples and repetitions / measurements. The difference is given by elastic modulus for the adhesive in use, and corresponding CZM damage parameters to capture the collapse condition of experiments.

It can be clearly seen a rather uniform load-bearing response for all the tested samples, with a mostly linear elastic behaviour and a typically brittle collapse mechanism that was also observed during the experimental campaign (see for example Fig. 8(b)).

In terms of load-bearing capacity and service class for joints with polyurethane or epoxy glue bonds, it is also possible to see the severe degradation of load-bearing capacity for a given setup / arrangement, as the moisture content increases. Figs. 11 and 12 emphasize the expected variation in maximum force and slip modulus, where numerical results for each configuration are compared to the response parameter (maximum axial force F_{ax} or slip modulus K_{ser}) calculated for the same geometrical condition under 9 % moisture content.

This means that specific calibration of input mechanical properties is needed to reproduce the failure mechanism of bonding lines. Further, this finding suggests that the actual operational conditions should be properly taken into account for design considerations.

In terms of damage configuration, see Fig. 13, the numerical analysis resulted in cohesive debonding at the CZM interface which was found in qualitative good agreement with experimental outputs as in Fig. 8(b). The non-dimensional CSDMG damage parameter is also shown to capture the evolution and distribution of cohesive debonding for selected loading conditions (25 % and 100 % of the maximum axial load F_{ax} taken up by a given BiR joint).

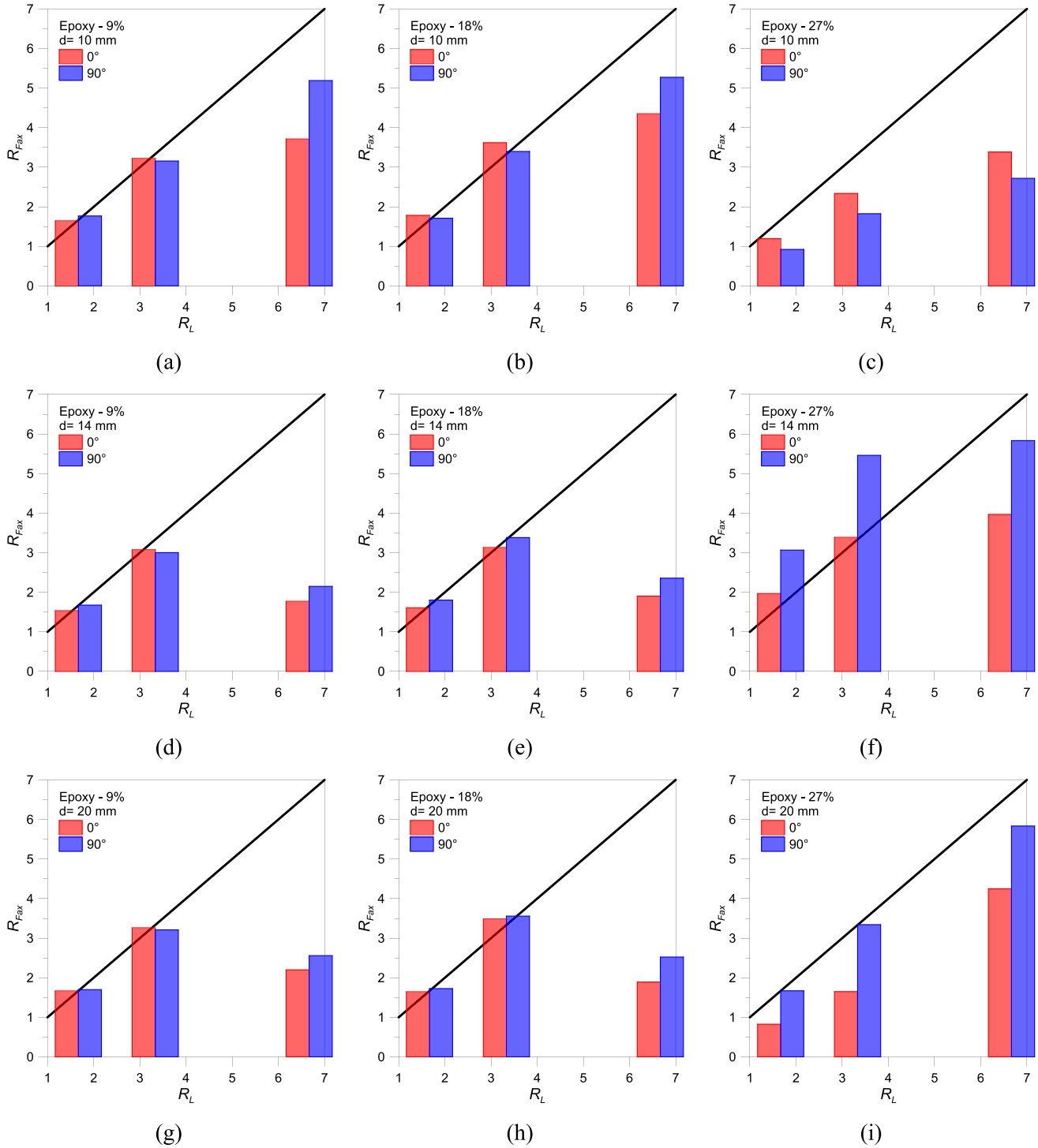

Fig. 16. Non-dimensional variation of maximum force (F_{ax}) with bond length, rod diameter and moisture content (epoxy adhesive, ABAQUS).

5.2. Numerical parametric study

The parametric investigation was carried out on based on adaptation of experimentally validated FE models from Section 5.1.

More precisely, a total of 144 BiR configurations was analyzed under pull-out setup. The set of connections was defined on the base of literature experiments, as well as design recommendations and practical applications of BiR connections for timber structures. As such, the numerical investigation included FE models for samples characterized by: (i) two adhesive types (polyurethane, epoxy); (ii) three moisture contents (9 %, 18 %, 27 %), (iii) two grain orientations for timber (parallel – $\alpha = 0°$, perpendicular – $\alpha = 90°$), (iv) variations in screw / anchorage length ($L = 60$ mm, 100 mm, 200 mm, 400 mm); (v) variations in screw diameter ($d = 10$ mm, 14 mm, 20 mm).

In doing so, material properties were taken from Section 5.1. Moreover, the thickness of adhesive bond was kept fix in $t_{adh} = 2$ mm, as in the past experiments. The mechanical calibration of elastic modulus for the adhesive in use and the corresponding moisture content / grain orientation was kept fix, while imposing modifications in rod diameter and anchorage length.

Also in terms of CZM-contact input properties, no modifications were undertaken when changing the rod diameter and anchorage length. In

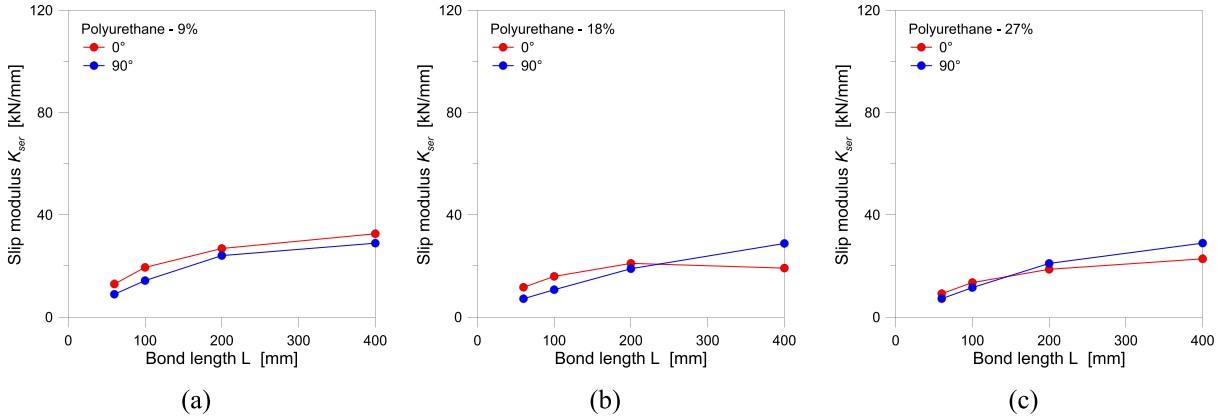

Fig. 17. Example of variation of slip modulus (K_{ser}) with bond length and moisture (polyurethane adhesive), with $d = 10$ mm, $L = 100$ mm, $t_{adh} = 2$ mm (ABAQUS).

this regard, the attention was primarily focused on the elastic stiffness and maximum load-bearing axial force of selected configurations, and this goal minimizes any possible influence from the use of du input parameters calibrated for collapse of models from Section 4.2. At the same time, it is recognized that possible modifications in the examined setup and testing conditions, or a more in depth analysis of failure brittleness and its possible sensitivity (in ultimate conditions) to geometric features of rods (especially the anchorage length), would necessarily require additional experimental support for a more precise d_u calibration.

For the discussion of parametric results, the load-bearing performance of samples from Section 5.1 was taken as a reference when varying the geometrical properties of anchorage length.

As far as the elastic and damage parameters for adhesives in use can be affected by operational conditions, a modification of load-bearing capacity for the BiR connections as a whole can be also expected. As such, each set of samples was compared to the 9 % moisture condition.

5.3. Mechanical performance

A first comparative attempt was carried out in terms of load-bearing mechanical parameters for the whole set of examined samples. Fig. 14 collects a summary of maximum axial force and slip modulus values for FE models grouped by type of glue.

The attention is given to grain orientation ($\alpha = 0°$ or 90°), for the full set of samples. It is possible to see, in this sense, that most of epoxy specimens offered best mechanical performance with bonding in parallel direction to the grain, both in terms of axial force and stiffness. In case of polyurethane samples, major scatter is shown in terms of axial force with grain orientation, while a generally higher slip modulus was predicted for samples with bonding parallel to the grain of timber.

5.4. Maximum force and service class

The effect of adhesive mechanical degradation as a consequence of moisture content variation was successively addressed in terms of a more quantitative analysis of maximum load-bearing capacity, that is the axial force peak taken up by each sample.

According to Eq. (1), the increase of screw / anchorage length L should ideally manifest in a directly proportional increase of load-bearing capacity.

For the discussion of parametric numerical results, the bond length $L = 60$ mm (and the corresponding axial force F_{ax}) was hence used as a reference configuration to quantify the effects of adhesive properties under different moisture content. In this sense, the discussion of parametric results in Figs. 15 and 16 is proposed in terms of:

$$R_{Fax} = \frac{(F_{ax})_i}{(F_{ax})_{L=60}} \tag{3}$$

and.

$$R_L = \frac{(L)_i}{(L)_{L=60}} \tag{4}$$

The diagonal trend in Figs. 15 and 16 represents the expected load-bearing capacity increase with bond length increase (from Eq. (1)).

It can be seen that the majority of numerical predictions are below the analytical trend. This is the case of both polyurethane and epoxy bonds, for all the examined diameters, and especially for long rods or in general for higher moisture content. This finding confirms that service conditions for adhesive bonds can be critical in BiR connections. At the same time, analytical or simplified calculations that disregard this possible material degradation are on the unsafe side, compared to numerical observations. Most importantly, no modification was numerically observed in the failure mechanism of the examined joints, with a rather close correlation to the experimental findings in Fig. 8, as well as with the numerical outcomes summarized in Fig. 13.

Overall, maximum degradation in terms of axial force was calculated for BiR connection based on polyurethane glue, compared to epoxy bonds.

5.5. Slip modulus and service class

The attention was successively focused on trends of slip modulus for the explored configurations. As far as a given geometry set is taken into account, for example, moisture increase can be quantified with stiffens modifications as in the example of Fig. 17.

A more detailed analysis of results is thus proposed in Figs. 18 and 19, where slip modulus values are compared to the prediction of samples under identical moisture content and $L = 60$ mm. As in Section 5.4, the diagonal plot denotes an ideal linear increase of slip modulus with the anchorage length of samples.

It is possible to note that polyurethane samples showed higher sensitivity of slip modulus with long screws and high moisture content (Fig. 18). Bondlines in the direction perpendicular to grain (90°), in this sense, gave evidence of higher stiffness for samples with long screws.

In case of epoxy bonded samples (Fig. 19), similar trends were collected for moisture variation, but less pronounced degradation with screw length, which suggests an improved / safer mechanical performance of BiR joints based on epoxy glue rather than polyurethane.

5.6. Maximum stress and service class

The calculation of stress peaks was finally addressed for all the

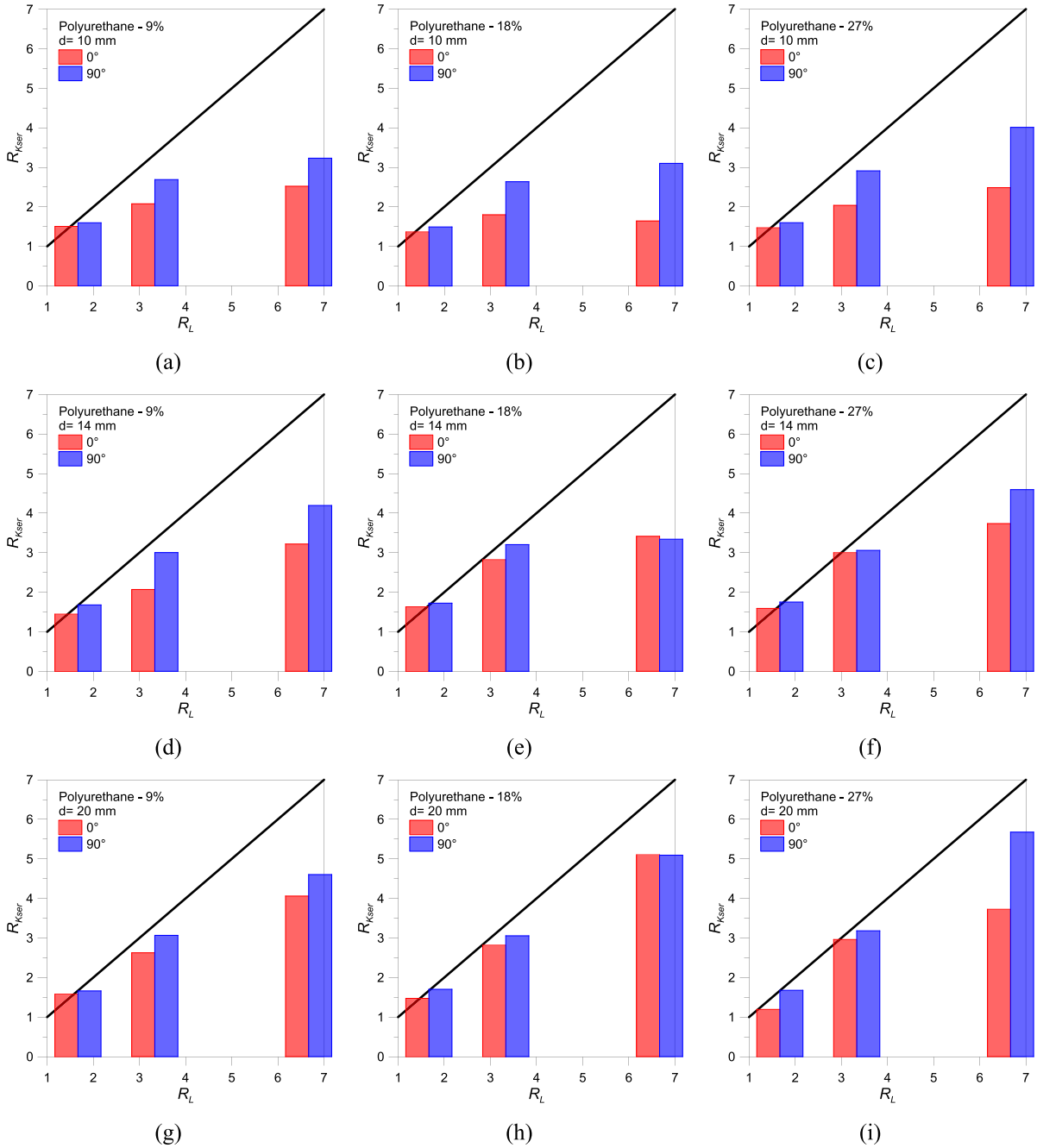

Fig. 18. Non-dimensional variation of slip modulus (K_{ser}) with bond length, rod diameter and moisture content (polyurethane adhesive, ABAQUS).

explored bondlines. Assuming that under the hypothesis of uniform distribution in the bond line the stress peak can be quantified as in Eq. (2), the analysis of parametric ultimate loads F_{ax} was focused on two different calculations.

First, a semi-analytical stress peak value was calculated based on $F_{ax} = F_{ax\_ABAQUS}$ in Eq. (2), that is:

$$\sigma_{max} = \frac{F_{ax\_ABAQUS}}{A_{bond}} \tag{5}$$

The typical example can be seen in Fig. 20(a) (selection).

At a second stage, the use of refined FE models was taken into account for a more detailed calculation of stress peaks in each examined bondline, based on available stress measurements for all the solid brick elements. More precisely, this second approach was based on the availability of a large number of brick solid elements to describe the nominal geometry of adhesive layers for the 144 configurations. The number of solid brick elements was calculated in the order of n_{el} = 4,000–5,000 for L = 60 mm and n_{el} = 8,000–12,000 for L = 400 mm screws for 1/4th specimen size as in Fig. 9 (with n_{el} variations depending on screw diameter). For each time increment of analysis, the principal stress in all these brick elements was separately calculated as a function of imposed vertical displacement / measured axial force in sample. The total number of stress plots (n_{el} plots for each examined configuration) was post-processeed to derive the average stress evolution in the whole bondline. The corresponding result is shown in Fig. 20(b), for selected samples. The so-calculated stress trends were further elaborated to express the maximum stress in bondline at different loading levels, namely 100 % (collapse), 75 %, 50 % and 25 % of the calculated F_{ax} value.

As far as the two calculation approaches as in Fig. 20(a) and (b) are taken into account, the accuracy of uniform stress distribution in

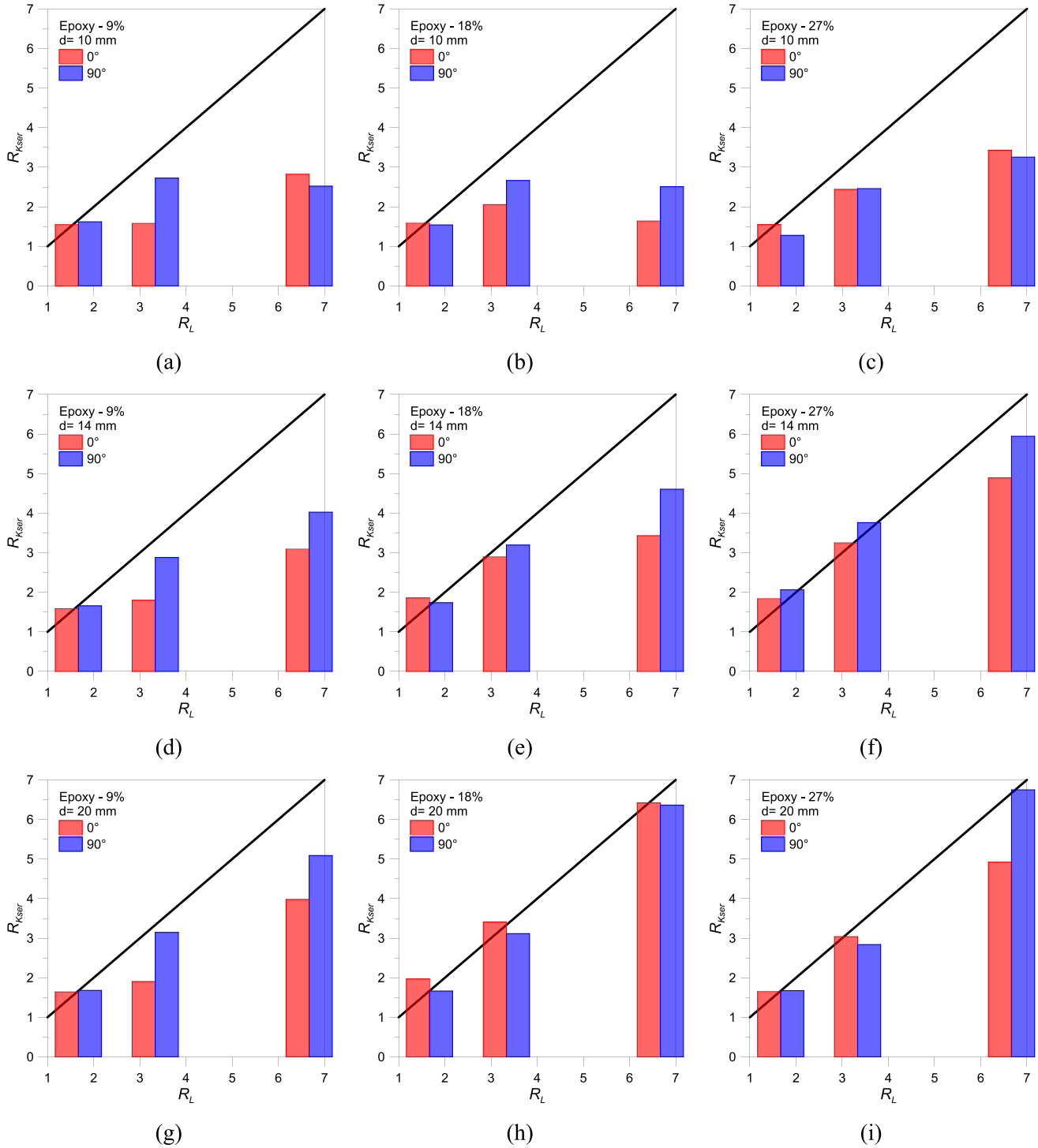

Fig. 19. Non-dimensional variation of slip modulus (K_{ser}) with bond length, rod diameter and moisture content (epoxy adhesive, ABAQUS).

bondlines can be addressed for various mechanical and operational conditions.

In this sense, Figs. 21 and 22 give evidence of comparative findings for BiR joints with polyurethane or epoxy glue respectively. For sake of clarity, BiRs with $L = 100$ mm or 200 mm are presented only.

It is possible to note that the use of Eq. (2) at near collapse condition is rather unsafe for the examined connections. The parametric charts for 100 % F_{ax} are in fact characterized by numerical dots that are distributed in the lower region of diagram / below diagonal. A similar trend was observed for both polyurethane and epoxy glued samples.

For lower axial loading levels, it can be seen in Figs. 21 and 22 that the set of comparative dots moved progressively towards the upper region of diagrams, which confirms the accuracy of uniform stress calculations as in Eq. (2) for rather elastic stages of mechanical performances. Most importantly, a more pronounced scatter in distribution of dots can be seen for the elastic stage of polyurethane or epoxy bonded samples, where the first type of connections is characterized by lower stress peaks than epoxy samples.

6. Conclusions

In this paper, the pull-out performance of Bonded-in-Rod (BiR) joints

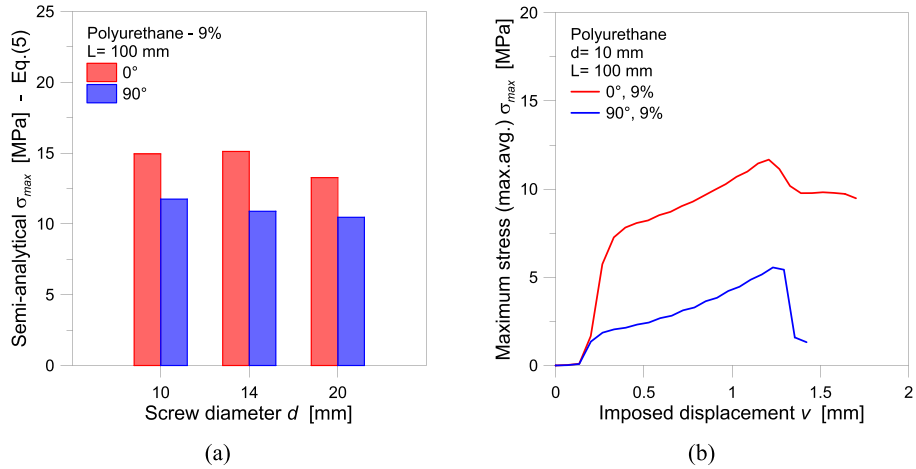

Fig. 20. Maximum stress analysis in the bondline: (a) example of rod and grain orientation effect or (b) example of refined element-based stress evolution, as a function of the imposed vertical displacement (ABAQUS).

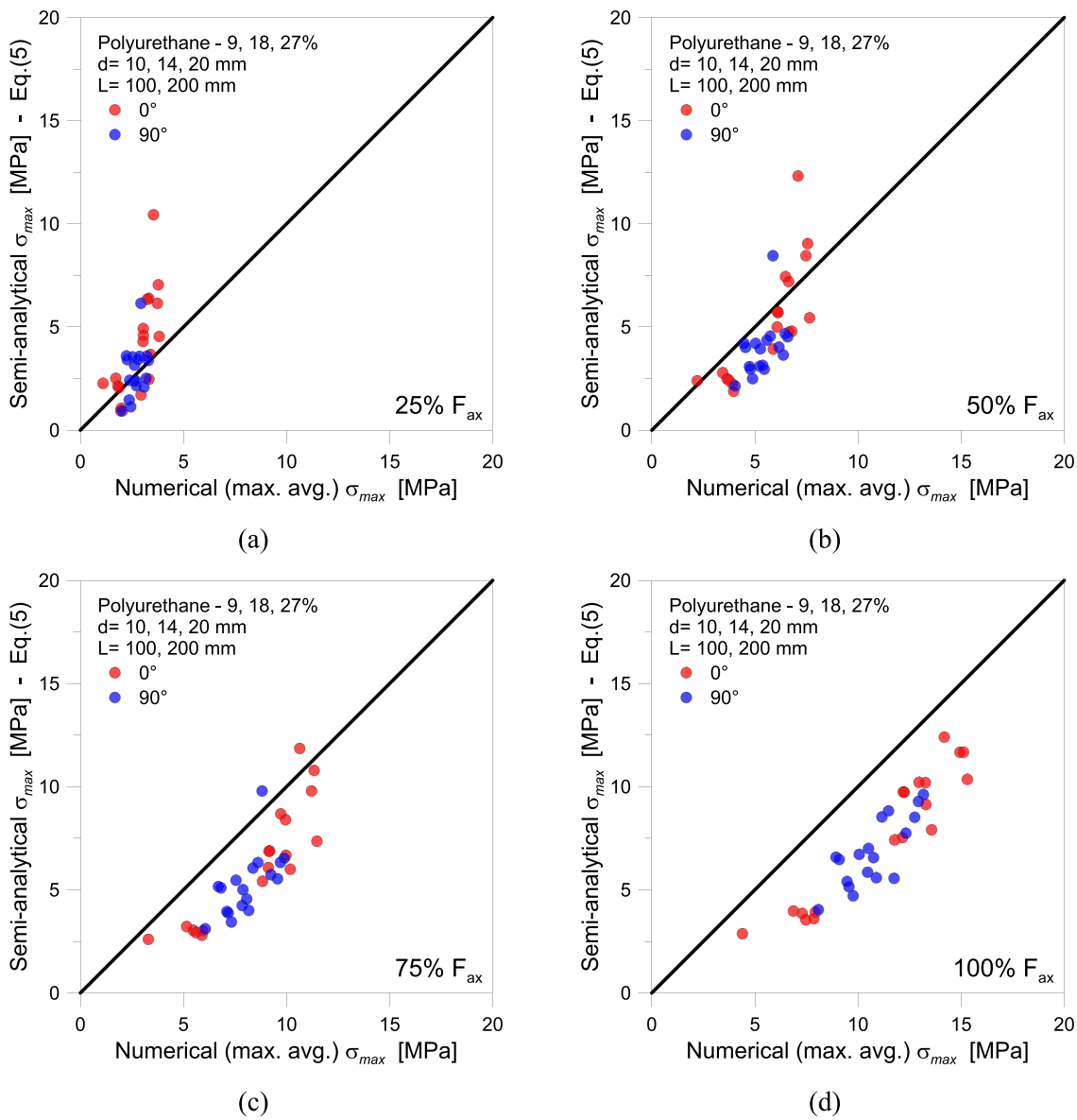

Fig. 21. Maximum stress in the bond line, for different loading levels (polyurethane, ABAQUS).

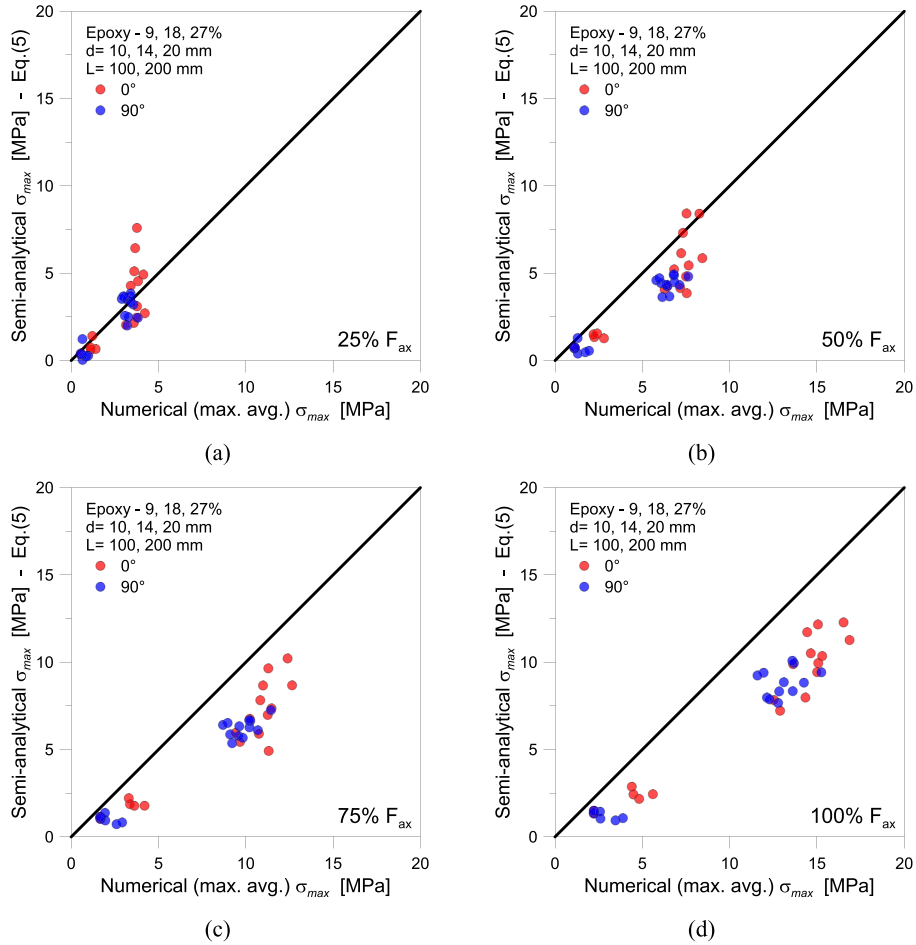

Fig. 22. Maximum stress in the bond line, for different loading levels (epoxy, ABAQUS).

for timber structures was explored with the support of Cohesive Zone Modelling (CZM) based Finite Element (FE) numerical models validated to past experiments. A wide set of geometrical and mechanical configurations, including 144 different samples, was numerically analyzed in terms of expected load-bearing capacity and collapse mechanism under different service classes (i.e., moisture content of 9, 18, 27 %).

In general terms, the analysis of BiR performances under different service conditions showed that for service class 1 no marked sensitivity was found with respect to the type of glue in use. Specimens with polyurethane adhesive showed higher capacity then specimens with epoxy, but in any case, a linear behaviour with brittle fracture was achieved. For service class 2, no marked modifications were found in terms of collapse mechanism. However, a substantial decrease of load-bearing capacity was measured. Finally, for service class 3, a huge drop in load-bearing capacity was found especially for epoxy bonded specimens (even down to − 50 % of maximum axial force).

The most important achievement of this extensive numerical research is fact that the increase of anchorage length was not associated to a directly proportional increase of load-bearing capacity in all the tested samples, as a major result of local damage occurrence and degradation of CZM interaction parameters.

Worth to note is also that the calculation of stress peaks in the bondline was generally found rather uniform in the adhesive layers, but typically lower (in maximum average terms) compared to analytical estimates, especially for loading levels up to (or over) the 60 % of load-bearing capacity.

The numerical investigation proved to be a significant tool in the research of the BiRs. However, considering BiR a modern type of connection that is gaining more and more momentum in significant timber structures, it is necessary to make a systematic test investigation in order to take into account all the stated conclusions for application in the standard. This should be especially applying to further testing of samples with different rod diameters (from 10 mm to the maximum of 20 mm) in combination with longer (from the shortest to the longest allowed length, in steps of 100 mm) anchoring lengths of bonded-in rods.

Declaration of Competing Interest

The authors declare that they have no known competing financial interests or personal relationships that could have appeared to influence the work reported in this paper.

Acknowledgments

The EU-COST Action CA18120 “CertBond” is gratefully acknowledged for providing financial support for a Short Term Scientific Mission (C.B. visitor at University of Zagreb, Croatia).

Annex

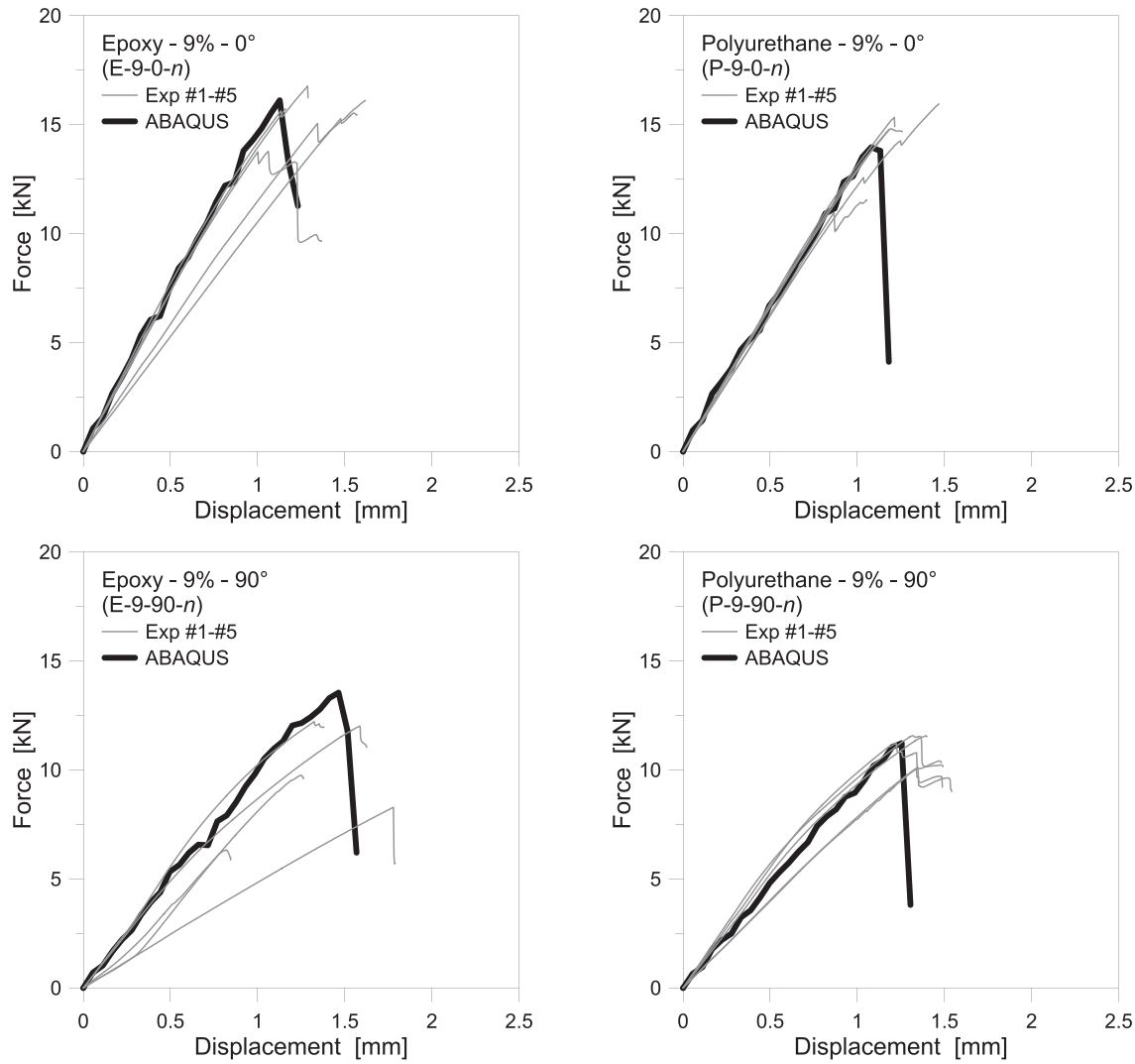

Fig. A1. FE model calibration for BiR connections (L= 60 mm, d= 10 mm, t_{adh}= 2 mm) – 9 % moisture (ABAQUS).

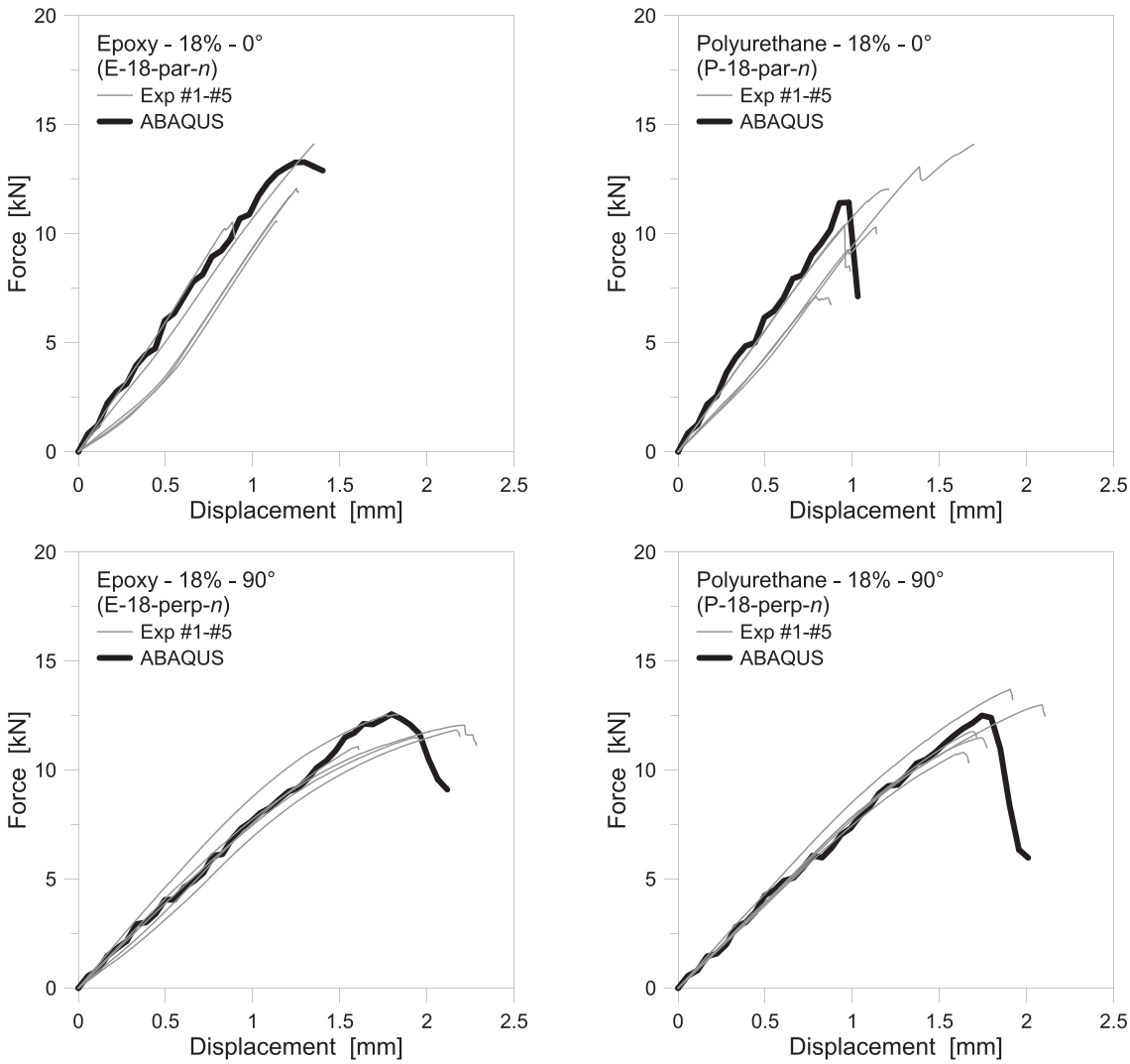

Fig. A2. FE model calibration for BiR connections (L= 60 mm, d= 10 mm, t_{adh}= 2 mm) – 18 % moisture (ABAQUS).

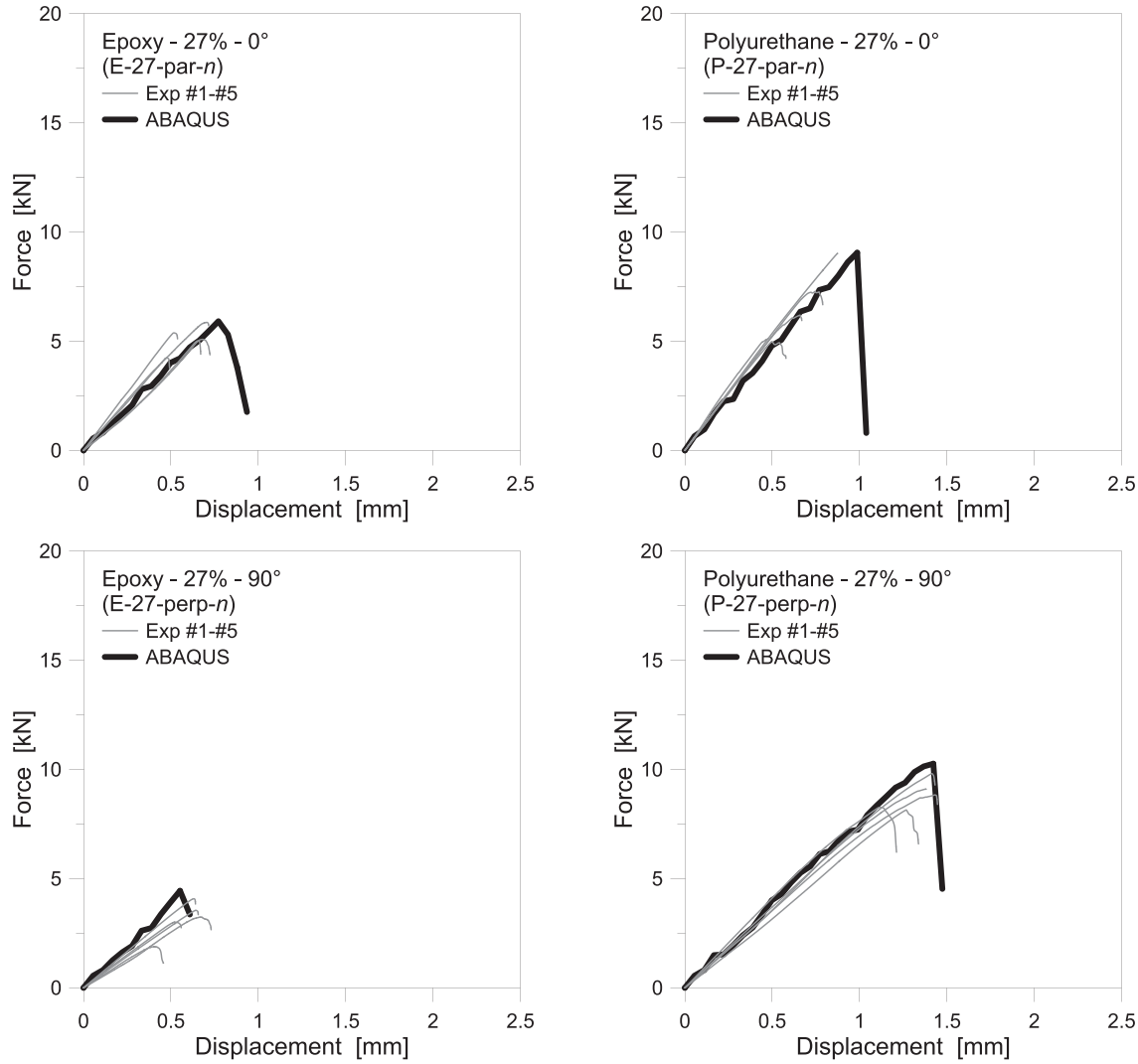

Fig. A3. FE model calibration for BiR connections (L= 60 mm, d= 10 mm, t_{adh}= 2 mm) – 27 % moisture (ABAQUS).

References

[1] Drass M.; Schober K.-U.; Kuechler M. Advancement of glued-in rods using polymer concrete as composite material. Axially-symmetric cracks. *Proceedings of World Conference on Timber Engineering, WCTE 2014, Quebec City, QC, Canada, 2014*.

[2] De Lorenzis L, Scialpi V, La Tegola A. Analytical and experimental study on bonded-in CFRP bars in glulam timber. Compos B Eng 2005;36:279–89. https://doi.org/10.1016/j.compositesb.2004.11.005.

[3] Chans DO, Cimadevila JE, Gutiérrez EM. Model for predicting the axial strength of joints made with glued-in rods in sawn timber. Constr Build Mater 2010;24:1773–8. https://doi.org/10.1016/j.conbuildmat.2010.02.010.

[4] Fava G, Carvelli V, Poggi C. Pull-out strength of glued-in FRP plates bonded in glulam. Constr Build Mater 2013;43:362–71. https://doi.org/10.1016/j.conbuildmat.2013.02.035.

[5] Gonzales E, Tannert T, Vallee T. The impact of defects on the capacity of timber joints with glued-in rods. Int J Adhes Adhes 2016;65:33–40. https://doi.org/10.1016/j.ijadhadh.2015.11.002.

[6] Yeboah D, Taylor S, McPolin D. Experimental study of interfacial stress distribution of bonded-in BFRP rod glulam joints using fibre optic sensors (FOS). Structures 2016;8:53–62. https://doi.org/10.1016/j.istruc.2016.08.006.

[7] Yeboah D, Taylor S, McPolin D, Gilfillan R. Pull-out behaviour of axially loaded basalt fibre reinforced polymer (BFRP) rods bonded perpendicular to the grain of glulam elements. Constr Build Mater 2013;38:962–9. https://doi.org/10.1016/j.conbuildmat.2012.09.014.

[8] Di Maria V, D'Andria L, Muciaccia G, Ianakiev A. Influence of elevated temperature on glued-in steel rods for timber elements. Constr Build Mater 2017;147:457–65. https://doi.org/10.1016/j.conbuildmat.2017.04.038.

[9] Madhoushi M, Ansell MP. Effect of glue-line thickness on pullout behavior of gluedin GFRP rods in LVL: Finite element analysis. Polym Test 2017;62:196–202. https://doi.org/10.1016/j.polymertesting.2017.06.029.

[10] Ratsch N, Böhma S, Voß M, Kaufmann M, Vallée T. Influence of imperfections on the load capacity and stiffness of glued-in rod connections. Constr Build Mater 2019;226:200–11. https://doi.org/10.1016/j.conbuildmat.2019.07.278.

[11] Kohl D, Ratsch N, Böhma S, Voß M, Kaufmann M, Vallée T. Influence of manufacturing methods and imperfections on the load capacity of glued-in rods. J Adhes 2018:1–22. https://doi.org/10.1080/00218464.2018.1508351.

[12] Ling Z, Yang H, Liu W, Zhu S, Chen X. Local bond stress-slip relationships between Glue laminated timber and epoxy bonded-in GFRP rod. Constr Build Mater 2018;170:1–12. https://doi.org/10.1016/j.conbuildmat.2018.03.052.

[13] Azinovic B, Danielsson H, Serrano E, Kramar M. Glued-in rods in cross laminated timber – Numerical simulations and parametric studies. Constr Build Mater 2019;212:431–41. https://doi.org/10.1016/j.conbuildmat.2019.03.331.

[14] Muciaccia M. An experimental approach to determine pull-outstrength of single and multiple axially loaded steel rods bonded in glulam parallel to the grain. Wood Mat Sci Eng 2019;14(2):88–98. https://doi.org/10.1080/17480272.2017.1404491.

[15] Grunwald C, Kaufman M, Alter B, Vallée T, Tannert T. Numerical investigations and capacity prediction of G-FRP rods glued into timber. Compos Struct 2019;202:47–59. https://doi.org/10.1016/j.compstruct.2017.10.010.

[16] Grunwald C, Vallée T, Fecht S, Bletz-Mühldorfer O, Diehl F, Bathon L, et al. Rods glued in engineered hardwood products part I: Experimental results under quasi-static loading. Int J Adhes Adhes 2019;90:163–81. https://doi.org/10.1016/j.ijadhadh.2018.05.003.

[17] Grunwald C, Vallée T, Fecht S, Bletz-Mühldorfer O, Diehl F, Bathon L, et al. Rods glued in engineered hardwood products part II: Numerical modelling and capacity prediction. Int J Adhes Adhes 2019;90:182–98. https://doi.org/10.1016/j.ijadhadh.2018.05.004.

[18] Orlando N, Taddia Y, Benvenuti E, Pizzo B, Alessandri C. End-repair of timber beams with laterally-loaded glued-in rods: Experimental trials and failure prediction through modelling. Constr Build Mater 2019;195:623–37. https://doi.org/10.1016/j.conbuildmat.2018.11.045.

[19] Khelifa M, Oudjene M, Ben ES, Rahim M. FE stress analysis and prediction of the pull-out of FRP rods glued into glulam timber. Wood Mat Sci Eng 2020;17:53–62. https://doi.org/10.1080/17480272.2020.1776769.
[20] Steiger R, Serrano E, Stepinac M, Rajcic V, O'Neill C, McPolin D, et al. Strengthening of timber structures with glued-in rods. Constr Build Mater 2015;97:90–105. https://doi.org/10.1016/j.conbuildmat.2015.03.097.
[21] Rajcic V.; Bjelanovic A.; Rak M. Comparison of the Pull-out Strength of Steel Bars Glued in Glulam Elements Obtained Experimentally and Numerically. *Proceedings of the CIB-W18 Timber Structures, Meeting 39, Florence, Italy, 2006*.
[22] Stepinac M.; Hunger F.; Tomasi R.; Serrano E.; Rajcic V.; Van de Kuilen J.W.G. Comparison of design rules for glued-in rods and design rule proposal for implementation in European standards. *Proceedings of the CIB-W18 Timber Structures, Meeting 46, Vancouver, BC, Canada*, 2013.
[23] Titirla MD, Michel L, Ferrier E. Mechanical behaviour of gluedin rods (carbon and glass fibre-reinforced polymers) for timber structures - An analytical and experimental study. Compos Struct 2019;208:70–7. https://doi.org/10.1016/j.compstruct.2018.09.101.
[24] Stepinac M.; Rajcic V.; Koscak J.; Damjanovic D. Assessment of the pull-out strength of glued-in rods with different test methods. *Proceedings of the World Conference on Timber Engineering, Vienna, Austria, 2016*.
[25] Buchanan AH. Timber Design Guide. Wellington, New Zealand: New Zealand Timber Industry Federation Inc.; 2011.
[26] DIN. Eurocode 5: Design of timber structures - Part 1-1: General - Common rules and rules for buildings - German version (DIN EN 1995-1-1:2010-12/A2:2014-07). *German Institute for Standardisation, Berlin, Germany, 2014*.
[27] Bsi. Eurocode 5: Design of timber structures - Part 1–1: General - Common rules and rules for buildings - UK version (BS EN 1995-1-1: 2004 +A2: 2014). London, United Kingdom: British Standards Institution; 2014.
[28] Serrano E. Glued-in rods for timber structures — a 3D model and finite element parameter studies. Int J Adhes Adhes 2001;21(2):115–27. https://doi.org/10.1016/S0143-7496(00)00043-9.
[29] Barbalic J, Rajcic V, Bedon C, Budzik MK. Short-Term Analysis of Adhesive Types and Bonding Mistakes on Bonded-in-Rod (BiR) Connections for Timber Structures. Appl Sci 2021;11(2665):1–18. https://doi.org/10.3390/app11062665.
[30] CEN/TC 250 SC 5: SC5.T5 N 1483 - Final BGD Connections - Bonded-in-rods - Background document. *European Committee for Standardization, Brussels, Belgium, 2021*.
[31] CEN. Eurocode - Basis of structural design (EN 1990:2002+A1:2005+AC:2008). *European Committee for Standardization, Brussels, Belgium, 2008*.
[32] CEN. Eurocode 5: Design of timber structures - Part 1-1: General - Common rules and rules for buildings (EN 1995-1-1:2004/A2:2014) *European Committee for Standardization, Brussels, Belgium, 2014*.
[33] CEN/TC 250 SC 5: Glued-in Rods in Glued Structural Timber Products - Testing, Requirements and Bond Shear Strength Classification (prEN 17334). *European Committee for Standardization, Brussels, Belgium, 2018*.
[34] CEN. Timber structures - Glued laminated timber and glued solid timber - Requirements (EN 14080:2013). *European Committee for Standardization, Brussels, Belgium, 2013*.
[35] CEN. Timber structures - Laminated veneer lumber (LVL) - Requirements (EN 14374:2006). *European Committee for Standardization, Brussels, Belgium, 2016*.
[36] CEN. Timber structures - Cross laminated timber - Requirements (EN 16351:2015). *European Committee for Standardization, Brussels, Belgium, 2015*.
[37] CEN. Wood-based panels for use in construction - Characteristics, evaluation of conformity and marking (EN 13986:2004+A1:2015). *European Committee for Standardization, Brussels, Belgium, 2015*.
[38] CEN. Fasteners - Mechanical properties of corrosion-resistant stainless steel fasteners - Part 1: Bolts, screws and studs with specified grades and property classes (EN ISO 3506-1:2020). *European Committee for Standardization, Brussels, Belgium, 2020*.
[39] CEN. Timber structures - Dowel-type fasteners - Requirements (EN 14592:2008). *European Committee for Standardization, Brussels, Belgium, 2008*.
[40] CEN. Mechanical properties of fasteners made of carbon steel and alloy steel - Part 1: Bolts, screws and studs with specified property classes - Coarse thread and fine pitch thread (ISO 898-1:2013; EN ISO 898-1:2013). *European Committee for Standardization, Brussels, Belgium, 2013*.
[41] Barenblatt GI. The formation of equilibrium cracks during brittle fracture. General ideas and hypotheses. Axially-symmetric cracks. J Appl Math Mech 1959;23:434–44. https://doi.org/10.1016/0021-8928(59)90157-1.
[42] Barenblatt GI. The Mathematical Theory of Equilibrium Cracks in Brittle Fracture. Adv Appl Mech 1962;7:55–129. https://doi.org/10.1016/S0065-2156(08)70121-2.
[43] Dugdale DS. Yielding of steel sheets containing slits. J Mech Phys Solids 1960;8:100–4. https://doi.org/10.1016/0022-5096(60)90013-2.
[44] Hillerborg A, Modéer M, Petersson PE. Analysis of crack formation and crack growth in concrete by means of fracture mechanics and finite elements. Cem Concr Res 1976;6:773–82. https://doi.org/10.1016/0008-8846(76)90007-7.
[45] Needleman A. A continuum model for void nucleation by inclusion debonding. J Appl Mech Trans ASME 1987;54:525–31. https://doi.org/10.1115/1.3173064.
[46] Cui W, Wisnom MR. A combined stress-based and fracture-mechanics-based model for predicting delamination in composites. Composites 1993;24(6):467–74. https://doi.org/10.1016/0010-4361(93)90016-2.
[47] Lammerant L, Verpoest I. Modelling of the interaction between matrix cracks and delaminations during impact of composite plates. Compos Sci Technol 1996;53:1171–8. https://doi.org/10.1016/S0266-3538(96)00071-1.
[48] Petrossian Z, Wisnom MR. Prediction of delamination initiation and growth from discontinuous plies using interface elements. Compos A Appl Sci Manuf 1998;29:503–15. https://doi.org/10.1016/S1359-835X(97)00134-6.
[49] Panigrahi SK, Pradhan B. Three dimensional failure analysis and damage propagation behavior of adhesively bonded single lap joints in laminated FRP composites. J Reinf Plast Compos 2007;26:183–201. https://doi.org/10.1177/0731684407070026.
[50] Bedon C.; Machalicka K.; Eliasova M.; Vokac M. Numerical modelling of adhesive connections including cohesive damage. In: *Challenging Glass 6, Vol. 6, 2018*. DOI: 10.7480/cgc.6.2155.
[51] Tserpes K, Barroso-Caro A, Carraro PA, Carrillo BV, Floros I, Gamon W, et al. A review on failure theories and simulation models for adhesive joints. J Adhes 2021:1–61. https://doi.org/10.1080/00218464.2021.1941903. ahead of print,.
[52] da Silva L.F.M.; Campilho R.D.S.G. Advances in Numerical Modeling of Adhesive Joints. In: *Advances in Numerical Modeling of Adhesive Joints. SpringerBriefs in Applied Sciences and Technology, 2012*. Springer, Berlin, Heidelberg. DOI: 10.1007/978-3-642-23608-2_1.
[53] Alfano G, Crisfield MA. Finite element interface models for the delamination analysis of laminated composites: Mechanical and computational issues. Int J Numer Meth Eng 2001;50:1701–36. https://doi.org/10.1002/nme.93.
[54] Allix O, Corigliano A. Modeling and simulation of crack propagation in mixed-modes interlaminar fracture specimens. Int J Fract 1996;77:111–40. https://doi.org/10.1007/BF00037233.
[55] Chen J. Predicting progressive delamination of stiffened fibre-composite panel and repaired sandwich panel by decohesion models. J Thermoplast Compos Mater 2002;15:429–42. https://doi.org/10.1177/089270570201500573 6.
[56] Chandra N, Li H, Shet C, Ghonem H. Some issues in the application of cohesive zone models for metal-ceramic interfaces. Int J Solids Struct 2002;39:2827–55. https://doi.org/10.1016/S0020-7683(02)00149-X.
[57] Kafkalidis MS, Thouless MD. The effects of geometry and material properties on the fracture of single lap-shear joints. Int J Solids Struct 2002;39:4367–83. https://doi.org/10.1016/S0020-7683(02)00344-X.
[58] Dias GF, de Moura MFSF, Chousal JAG, Xavier J. Cohesive laws of composite bonded joints under mode I loading. Compos Struct 2013;106:646–52. https://doi.org/10.1016/j.compstruct.2013.07.027.
[59] de Moura MFSF, Campilho RDSG, Gonçalves JPM. Pure mode II fracture characterization of composite bonded joints. Int J Solids Struct 2009;46:1589–95. https://doi.org/10.1016/j.ijsolstr.2008.12.001.
[60] Campilho RDSG, Banea MD, Neto JABP, Da Silva LFM. Modelling adhesive joints with cohesive zone models: Effect of the cohesive law shape of the adhesive layer. Int J Adhes Adhes 2013;44:48–56. https://doi.org/10.1016/j.ijadhadh.2013.02.006.
[61] Floros IS, Tserpes KI, Löbel T. Mode-I, mode-II and mixed-mode I+II fracture behavior of composite bonded joints: experimental characterization and numerical simulation. Compos B Eng 2015;78:459–68. https://doi.org/10.1016/j.compositesb.2015.04.006.
[62] Harper PW, Hallett SR. A fatigue degradation law for cohesive interface elements - Development and application to composite materials. Int J Fatigue 2010;32:1774–87. https://doi.org/10.1016/j.ijfatigue.2010.04.006.
[63] Kawashita LF, Hallett SR. A crack tip tracking algorithm for cohesive interface element analysis of fatigue delamination propagation in composite materials. Int J Solids Struct 2012;49:2898–913. https://doi.org/10.1016/j.ijsolstr.2012.03.034.
[64] Pirondi A, Nicoletto G. Mixed mode I/II fatigue crack growth in adhesive joints. Eng Fract Mech 2006;73:2557–68. https://doi.org/10.1016/j.engfracmech.2006.04.009.
[65] May M, Hallett SR. An advanced model for initiation and propagation of damage under fatigue loading - part I: model formulation. Compos Struct 2011;93:2340–9. https://doi.org/10.1016/j.compstruct.2011.03.022.
[66] Rocha AVM, Akhavan-Safar A, Carbas R, Marques EAS, Goyal R, El-zein M, et al. Numerical analysis of mixed-mode fatigue crack growth of adhesive joints using CZM. Theor Appl Fract Mech 2020;106(102493):1–28. https://doi.org/10.1016/j.tafmec.2020.102493.
[67] Floros I, Tserpes K. Fatigue crack growth characterization in adhesive CFRP joints. Compos Struct 2019;207:531–6. https://doi.org/10.1016/j.compstruct.2018.09.020.
[68] Bedon C, Fragiacomo M. Numerical analysis of timber-to-timber joints and composite beams with inclined self-tapping screws. Compos Struct 2019;207:13–28. https://doi.org/10.1016/j.compstruct.2018.09.008.
[69] Avez T, Descamps E, Serrano E, Léoskool L. Finite Element modelling of inclined screwed timber to timber connections with a large gap between the elements. Eur J Wood Wood Prod 2016;74:467–71. https://doi.org/10.1007/s00107-015-1002-1.
[70] Bedon C, Sciomenta M, Fragiacomo M. Correlation approach for the push-out and full-size bending short-term performances of timber-to-timber slabs with self-tapping screws. Eng Struct 2021;238:112232. https://doi.org/10.1016/j.engstruct.2021.112232.
[71] Bedon C, Fragiacomo M. Three-dimensional modelling of notched connections for timber-concrete composite beams. Struct Eng Int 2017;27(2):184–96. https://doi.org/10.2749/101686617X14881932435295.
[72] Bergstedt AE, Lyck C. Larch Wood – A literature review. Forest & LandscapeWorking Papers 2007;no. 23.
[73] CEN. General purpose adhesives for structural assembly - Requirements and test methods (EN 15274:2015). *European Committee for Standardization, Brussels, Belgium, 2015*.
[74] CEN. Timber Structures - Test methods - Withdrawal capacity of timber fasteners (EN 1382: 2016). Brussels, Belgium: European Committee for Standardization; 2016.